

# Over-the-Air Computation Based on Balanced Number Systems for Federated Edge Learning

Alphan Şahin, *Member, IEEE*

**Abstract**—In this study, we propose a digital over-the-air computation (OAC) scheme for achieving continuous-valued (analog) aggregation for federated edge learning (FEEL). We show that the average of a set of real-valued parameters can be calculated approximately by using the average of the corresponding numerals, where the numerals are obtained based on a balanced number system. By exploiting this key property, the proposed scheme encodes the local stochastic gradients into a set of numerals. Next, it determines the positions of the activated orthogonal frequency division multiplexing (OFDM) subcarriers by using the values of the numerals. To eliminate the need for precise sample-level time synchronization, channel estimation overhead, and channel inversion, the proposed scheme also uses a non-coherent receiver at the edge server (ES) and does not utilize a pre-equalization at the edge devices (EDs). We theoretically analyze the MSE performance of the proposed scheme and the convergence rate for a non-convex loss function. To improve the test accuracy of FEEL with the proposed scheme, we introduce the concept of adaptive absolute maximum (AAM). Our numerical results show that when the proposed scheme is used with AAM for FEEL, the test accuracy can reach up to 98% for heterogeneous data distribution.

**Index Terms**—Balanced numerals, federated learning, non-coherent over-the-air computation, quantization.

## I. INTRODUCTION

Over-the-air computation (OAC) refers to the computation of mathematical functions by exploiting the signal-superposition property of wireless multiple-access channels [2], [3]. To improve the utilization of limited wireless resources, it was initially considered for wireless sensor networks [4]. With the same motivation, OAC has recently gained increasing attention in the literature for applications such as distributed learning or wireless control systems [5]–[7]. For example, federated edge learning (FEEL), one of the promising distributed edge learning frameworks, aims to implement federated learning (FL) [8] over a wireless network. With FEEL, the task of model training is distributed across multiple edge devices (EDs) and the data uploading is avoided to promote user privacy [6], [9]. Instead of data samples, EDs share a large number of local stochastic gradients (or local model parameters) with an edge server (ES) for aggregation, e.g., averaging. However, typical orthogonal user multiplexing methods such as orthogonal frequency division multiple access (OFDMA) can be wasteful in this scenario since the ES may not be interested in the local information of the EDs but

only in a function of them. Similarly, a control system that requires an input that is a function of many Internet-of-Things (IoT) devices' readings can suffer from high latency since the available spectrum for these networks is often limited and the OAC can address the latency issues by calculating the functions, e.g., difference equations [7], over the air.

Although OAC is a promising concept to address the latency issues in the aforementioned use cases, it is challenging to realize a reliable OAC scheme under fading channels. This is because the typical equalization or phase correction methods used at the receiver for traditional multiple-access schemes, e.g., OFDMA, cannot be directly employed for OAC to compensate for the channel distortion or imperfect synchronization as the transmitted symbols are distorted by the channel before the signal superposition. To address this issue, a majority of the state-of-the-art OAC methods rely on pre-equalization techniques [10]–[17]. However, a pre-equalizer can impose stringent requirements on the underlying mechanisms such as time-frequency-phase synchronization, channel estimation, and channel prediction, which can be challenging to satisfy under non-stationary channel conditions [18], [19]. Most of the state-of-the-art OAC schemes use analog modulation schemes to achieve continuous-valued computation, e.g., [10], [20], and [21]. However, in fading channels, analog modulations can be more susceptible to noise as compared to digital schemes. Although there are digital methods, e.g., one-bit broadband digital aggregation (OBDA) [13] and frequency-shift keying (FSK)-based majority vote (MV) (FSK-MV) [22], these schemes do not allow one to compute a continuous-valued function. In this paper, as opposed to earlier work, we introduce an OAC scheme for FEEL, where the local stochastic gradients are encoded into a set of numerals based on a balanced (also called signed-digit) number system [23] to achieve a continuous-valued computation over a digital scheme.<sup>1</sup> The proposed method does not rely on pre-equalization and the availability of channel state information (CSI) at the EDs and the ES, leading to relaxed synchronization requirements as compared to the methods relying on the availability of the CSI at the EDs.

### A. Related Work

1) *Over-the-air computation*: In the literature, OAC schemes are particularly investigated to reduce the per-round communication latency of FEEL. In [10], broadband analog

<sup>1</sup>To avoid confusion, we use the terms "numeral" and "balanced" for "digit" and "signed-digit", respectively, since the term "digit" may specifically imply the ten symbols of the common base 10 numeral system.

Alphan Şahin is with the Electrical Engineering Department, University of South Carolina, Columbia, SC, USA. E-mail: asahin@mailbox.sc.edu

This paper in part was submitted to be presented at the IEEE Global Communication Conference (GLOBECOM) 2022 - Workshop on Wireless Communications for Distributed Intelligence [1].

aggregation (BAA) that modulates the orthogonal frequency division multiplexing (OFDM) subcarriers with the model parameters is proposed. To overcome the impact of the multipath channel on the transmitted signals, the symbols on the OFDM subcarriers are multiplied with the inverse of the channel coefficients and the subcarriers that fade are excluded from the transmissions, known as *truncated-channel inversion (TCI)* in the literature. In [11], an additional time-varying precoder is applied along with TCI to facilitate the aggregation. In [12], the gradient estimates are sparsified and the sparse vectors are projected into a low-dimensional vector to reduce the bandwidth. The compressed data is transmitted with BAA. In [15], the power control and re-transmissions for BAA over static channels are investigated to obtain the optimal number of re-transmissions. In [16], instead of TCI, the parameters are multiplied with the conjugate of the channel coefficients (i.e., maximum-ratio transmission) to increase the power efficiency. In [17], the channel inversion is optimized with the consideration of sum-power constraint to avoid potential interference issues. In [13], OBDA is proposed to facilitate the implementation of FEEL for a practical wireless system. In this method, considering distributed training by MV with the sign stochastic gradient descent (signSGD) [24], the EDs transmit quadrature phase-shift keying (QPSK) symbols along with TCI, where the real and imaginary parts of the QPSK symbols are formed by using the signs of the stochastic gradients. At the ES, the signs of the real and imaginary components of the superposed received symbols on each subcarrier are calculated to obtain the MV for the sign of each gradient. The authors in [25] also consider OBDA, but the pre-equalization in this method applies only phase correction to the transmitted symbols (i.e., equal-gain transmission) by emphasizing the fact that amplitude alignment is not needed for digital OAC. The reader is referred to [26] for various combining strategies for channel-aware decision fusion under the assumption of real-valued channel coefficients.

The methods relying on channel-inversion techniques require phase synchronization for coherent superposition. However, to achieve phase synchronization, a precise sample-level time synchronization at both EDs and ES needs to be maintained, which is very challenging in practice due to the synchronization impairments and inaccurate clocks at the radios [27]. Also, residual carrier frequency causes additional phase rotations [28]. To address these issues, in the literature, several OAC methods that do not use pre-equalization are proposed at the expense of more resource consumption. For example, in [29] and [30], the authors consider blind EDs, i.e., CSI is not available at the ED. By exploiting channel hardening, the ES utilizes an estimate of the superposed CSI to achieve an analog aggregation with maximum-ratio combining (MRC). In [22], [31], [32], and [33], the OAC for FEEL is realized by exploiting non-coherent receiver techniques. Similar to OBDA [13], the schemes in these studies depend on the distributed training by MV [24]. However, instead of modulating the phase of the OFDM subcarriers based on the sign of the local stochastic gradients, the schemes use various keying approaches such as FSK, pulse-position modulation (PPM), and chirp-shift keying (CSK) along with a non-

coherent comparator to detect the MV at the ES. While they can provide robustness against time variation of the wireless channel, synchronization errors, and imperfect power control, the 1-bit quantization nature of signSGD can degrade the test accuracy in heterogeneous data distribution scenarios. In [20] and [21], Goldenbaum and Stańczak propose to calculate the energy of a sequence of superposed symbols. In [34], they show that their scheme can also work when there is no CSI at the transmitter under a scenario where the ES is equipped with multiple antennas.

2) *Quantization*: In the literature, extensive efforts have been made to decrease the communication costs of machine learning algorithms by quantization. For example, in [35], a general quantized stochastic gradient descent (SGD) (QSGD) with the Elias integer encoding is investigated for encoding the gradients by relying on the fact that large gradients are often less frequent. The signSGD, proposed in [24], is an extreme case of quantization, where the signs of the gradients are considered for the training. In [36], a ternary quantization, which is a balanced number system where the base is 3, is applied to the model parameters to implement FL based on parameter averaging. In [37], by considering the trade-off between precision and energy, the quantization levels for the neural network parameters are optimized for FL. In [38], a gradient quantization method that uses the historical gradients as side information to compress the local gradients is proposed. The authors exploit the fact that gradients between adjacent rounds may have a high correlation for SGD. Nevertheless, these quantization methods consider either ideal communication channels for training or orthogonal multiple access for EDs. Also, they do not consider an OAC scheme.

## B. Contributions

The contributions of this study can be listed as follows:

**Continuous-valued OAC with a digital scheme:** We show that the average of a set of real-valued parameters can be calculated by using the average of the corresponding numerals in the real domain, approximately. By exploiting this key property, discussed in Section III-A, we achieve continuous-valued computation over a digital OAC scheme. With the proposed method, the EDs first encode the real-valued local stochastic gradients into the numerals for a given balanced number system. The EDs activate the dedicated time-frequency resources (i.e., OFDM subcarriers) based on the values of the numerals. The EDs simultaneously transmit their OFDM symbols and the average numerals are calculated at the ES with a non-coherent receiver. By using the average of the numerals, the ES computes an estimate of the real-valued average stochastic gradient. To the best of our knowledge, this is the first study that uses a general balanced number system for OAC.

**Theoretical MSE analysis:** We derive the classical mean squared error (MSE) and Bayesian MSE (BMSE) of the estimator of the average stochastic gradient for a given set of parameters such as the number of numerals, number of EDs, and number of antennas at the ES. By extending our initial work in [1], we introduce the concept of adaptive absolute

maximum (AAM), where each ED shares a single parameter with the ES to adjust the maximum quantization level to minimize the estimation error over the communication rounds of FEEL.

**Theoretical convergence analysis:** By using the MSE derivation and considering both homogeneous and heterogeneous data distributions in the network, we show the convergence of FEEL in the presence of the proposed scheme with and without AAM for a non-convex loss function, i.e., Theorem 1 and Theorem 2, respectively. While the proposed framework without AAM contributes to the noise ball due to the stochastic gradients, the impact is largely addressed when the proposed scheme is utilized with the AAM.

*Organization:* The rest of the paper is organized as follows. In Section II, the notation and the preliminary discussions used in the rest of the sections are provided. In Section III, the proposed OAC scheme and its MSE performance are discussed. In Section IV, the convergence rate of the FEEL with the proposed scheme is discussed. In Section V, the numerical results are provided. We conclude the paper in Section VI.

*Notation:* The sets of complex numbers, real numbers, integers, and integers modulo  $H$  are denoted by  $\mathbb{C}$ ,  $\mathbb{R}$ ,  $\mathbb{Z}$ , and  $\mathbb{Z}_H$  respectively. The  $N$ -dimensional all zero vector and the  $N \times N$  identity matrix are  $\mathbf{0}_N$  and  $\mathbf{I}_N$ , respectively. The function  $\mathbb{I}[\cdot]$  results in 1 if its argument holds, otherwise, it is 0.  $\mathbb{E}_x[\cdot]$  and  $\mathbb{E}[\cdot]$  are the expectation of its argument over  $x$  and the expectation of its argument over all random variables, respectively.  $\nabla f(\mathbf{w})$  denotes the gradient of the function  $f$ , i.e.  $\nabla f$ , at the point  $\mathbf{w}$ . The zero-mean circularly symmetric multivariate complex Gaussian distribution with the covariance matrix  $\mathbf{C}_M$  of an  $M$ -dimensional random vector  $\mathbf{x} \in \mathbb{C}^{M \times 1}$  is denoted by  $\mathbf{x} \sim \mathcal{CN}(\mathbf{0}_M, \mathbf{C}_M)$ . The gamma distribution with the shape parameter  $n$  and the rate  $\lambda$  is  $\Gamma(n, \lambda)$ . The binomial distribution with the  $K$  trials and the success probability  $p$  for each trial is  $\mathcal{B}(K, p)$ . The uniform distribution with the support between  $a$  and  $b$  is  $\mathcal{U}(a, b)$ . Normal distribution with mean  $\mu$  and variance  $\sigma^2$  is  $\mathcal{N}(\mu, \sigma^2)$ . The  $\ell_2$ -norm of the vector  $\mathbf{x}$  is  $\|\mathbf{x}\|_2$ .

## II. PRELIMINARIES AND SYSTEM MODEL

In this section, we provide the signal and learning model that we use throughout the paper and the preliminaries related to encoding and decoding based on a balanced number system.

### A. Signal Model

We consider a wireless network with  $K$  EDs that are connected to an ES, where each ED and the ES are equipped with a single antenna and  $R$  antennas, respectively. We assume that the large-scale impact of the wireless channel is compensated with a power control mechanism, e.g., closed-loop power control with the physical uplink control channel (PUCCH) in Fifth Generation (5G) New Radio (NR) [39], before the training process for FEEL begins.

For the signal model, we assume that the EDs access the wireless channel on the same time-frequency resources

*simultaneously* with  $S$  OFDM symbols consisting of  $M$  active subcarriers for OAC. Assuming that the cyclic prefix (CP) duration is larger than the sum of the maximum time-synchronization error and the maximum-excess delay of the channel, we express the superposed modulation symbols on  $R$  antennas at the ES for the  $l$ th subcarrier of the  $m$ th OFDM symbol for the  $\ell$ th communication round of the training, i.e.,  $\mathbf{r}_{l,m}^{(\ell)} \in \mathbb{C}^{R \times 1}$  as

$$\mathbf{r}_{m,l}^{(\ell)} = \sum_{k=0}^{K-1} \mathbf{h}_{k,m,l}^{(\ell)} t_{k,m,l}^{(\ell)} + \mathbf{n}_{m,l}^{(\ell)}, \quad (1)$$

where  $\mathbf{h}_{k,m,l}^{(\ell)} \sim \mathcal{CN}(\mathbf{0}_R, \mathbf{I}_R)$  is a  $R \times 1$  vector that consists of the channel coefficients between  $R$  antennas at the ES and the  $k$ th ED,  $t_{k,m,l}^{(\ell)} \in \mathbb{C}$  is the transmitted modulation symbol from the  $k$ th ED, and  $\mathbf{n}_{m,l}^{(\ell)} \sim \mathcal{CN}(\mathbf{0}_R, \sigma_n^2 \mathbf{I}_R)$  is a  $R \times 1$  additive white Gaussian noise (AWGN) vector, where  $\sigma_n^2$  is the noise variance for  $l \in \mathbb{Z}_M$  and  $m \in \mathbb{Z}_S$ . We denote the signal-to-noise ratio (SNR) of an ED at the ES receiver as  $1/\sigma_n^2$ .

In practice, the synchronization point where the discrete Fourier transform (DFT) starts to be applied to the received signal for demodulation at the ES and the time synchronization across the EDs may not be precise. To model former impairment, we assume that the synchronization point can deviate by  $N_{\text{err}}$  samples within the CP window. For the latter impairment, the time of arrivals of the EDs' signals at the ES location are sampled from a uniform distribution between 0 and  $T_{\text{sync}}$  seconds, where  $T_{\text{sync}}$  is equal to the reciprocal of the signal bandwidth. Note that the coarse time-synchronization can be maintained with the state-of-the-art protocols used in cellular systems. We introduce additional phase rotations to  $\mathbf{h}_{k,m,l}^{(\ell)}$  to capture the impact of the time-synchronization errors on  $\mathbf{r}_{m,l}^{(\ell)}$ . We assume that the frequency synchronization is handled before the transmissions with a control mechanism as done in 3GPP Fourth Generation (4G) Long Term Evolution (LTE) and/or 5G NR with random-access channel (RACH) and/or PUCCH [39] or custom methods such as AirShare [40].

### B. Learning Model

Let  $\mathcal{D}_k$  denote the local data set containing the labeled data samples  $(\mathbf{x}_\ell, y_\ell)$  at the  $k$ th ED,  $\forall k \in \mathbb{Z}_K$ , where  $\mathbf{x}_\ell$  is the  $\ell$ th data sample with its ground truth label  $y_\ell$ . Suppose that all EDs upload their data sets to the ES. The centralized learning problem can then be expressed as

$$\mathbf{w}^* = \arg \min_{\mathbf{w} \in \mathbb{R}^Q} F(\mathbf{w}) = \arg \min_{\mathbf{w} \in \mathbb{R}^Q} \frac{1}{|\mathcal{D}|} \sum_{\forall (\mathbf{x}_\ell, y_\ell) \in \mathcal{D}} f(\mathbf{w}; \mathbf{x}_\ell, y_\ell), \quad (2)$$

where  $F(\mathbf{w})$  is the loss function,  $\mathcal{D} = \mathcal{D}_0 \cup \mathcal{D}_1 \cup \dots \cup \mathcal{D}_{K-1}$  is the complete data set, and  $f(\mathbf{w}; \mathbf{x}_\ell, y_\ell)$  is the sample loss function for the parameters  $\mathbf{w} = [w_0, \dots, w_{Q-1}]^T \in \mathbb{R}^Q$ , and  $Q$  is the number of parameters. With (full-batch) gradient descent, a local optimum point can be obtained as

$$\mathbf{w}^{(\ell+1)} = \mathbf{w}^{(\ell)} - \eta \mathbf{g}^{(\ell)}, \quad (3)$$

where  $\eta$  is the learning rate and the gradient vector  $\mathbf{g}^{(\ell)} = [g_0^{(\ell)}, \dots, g_{Q-1}^{(\ell)}]^T \in \mathbb{R}^Q$  can be expressed as

$$\mathbf{g}^{(\ell)} = \nabla F(\mathbf{w}^{(\ell)}) = \frac{1}{|\mathcal{D}|} \sum_{\forall (\mathbf{x}_\ell, y_\ell) \in \mathcal{D}} \nabla f(\mathbf{w}^{(\ell)}; \mathbf{x}_\ell, y_\ell). \quad (4)$$

Equation (3) can be re-written as

$$\begin{aligned} \mathbf{w}^{(\ell+1)} &= \mathbf{w}^{(\ell)} - \eta \sum_{k=0}^{K-1} \frac{|\mathcal{D}_k|}{|\mathcal{D}|} \underbrace{\frac{1}{|\mathcal{D}_k|} \sum_{\forall (\mathbf{x}_\ell, y_\ell) \in \mathcal{D}_k} \nabla f(\mathbf{w}^{(\ell)}; \mathbf{x}_\ell, y_\ell)}_{\triangleq \mathbf{g}_k^{(\ell)}} \\ &= \sum_{k=0}^{K-1} \frac{|\mathcal{D}_k|}{|\mathcal{D}|} \left( \mathbf{w}^{(\ell)} - \eta \mathbf{g}_k^{(\ell)} \right), \end{aligned}$$

where  $\mathbf{g}_k^{(\ell)} \in \mathbb{R}^Q$  denotes the local gradient vector at the  $k$ th ED. Therefore, (3) can still be realized by communicating the local gradients or locally updated model parameters between the EDs and the ES, rather than moving the local data sets from the EDs to the ES, which is beneficial for promoting data privacy [6], [9]. This observation also shows the underlying principle of the plain FL based on gradient or model parameter aggregations [8].

FEEL aims to realize FL over a wireless network. In this study, we consider the implementation of FL based on SGD, known as FedSGD [8], over a wireless network: The  $k$ th ED calculates an estimate of the local gradient vector, denoted by  $\tilde{\mathbf{g}}_k^{(\ell)} = [\tilde{g}_{k,0}^{(\ell)}, \dots, \tilde{g}_{k,Q-1}^{(\ell)}]^T \in \mathbb{R}^Q$ , as

$$\tilde{\mathbf{g}}_k^{(\ell)} = \nabla F_k(\mathbf{w}^{(\ell)}) = \frac{1}{n_b} \sum_{\forall (\mathbf{x}_\ell, y_\ell) \in \tilde{\mathcal{D}}_k} \nabla f(\mathbf{w}^{(\ell)}; \mathbf{x}_\ell, y_\ell), \quad (5)$$

where  $\tilde{\mathcal{D}}_k \subset \mathcal{D}_k$  is the data batch obtained from the local data set and  $n_b = |\tilde{\mathcal{D}}_k|$  as the batch size. The EDs transmit the local gradient estimates to the ES. Assuming identical data set sizes across the EDs, to solve (2), the ES calculates the average stochastic gradient vector  $\mathbf{v}^{(\ell)} \triangleq [v_0^{(\ell)}, \dots, v_{Q-1}^{(\ell)}]^T = \frac{1}{K} \sum_{k=0}^{K-1} \tilde{\mathbf{g}}_k^{(\ell)}$  and broadcasts it to the EDs. Finally, the model parameters at the EDs are updated as

$$\mathbf{w}^{(\ell+1)} = \mathbf{w}^{(\ell)} - \eta \mathbf{v}^{(\ell)}. \quad (6)$$

With traditional orthogonal user multiplexing, the per-round communication latency for FEEL linearly increases with the number of EDs [41]. With the motivation of eliminating per-round communication latency, the main objective of this work is to calculate an estimate of  $\mathbf{v}^{(\ell)}$ , denoted by  $\hat{\mathbf{v}}^{(\ell)} \triangleq [\hat{v}_0^{(\ell)}, \dots, \hat{v}_{Q-1}^{(\ell)}]^T$ , through a digital OAC scheme robust against fading channels.

### C. Balanced Number Systems

We define  $f_{\text{enc},\beta}$  as a function that maps  $v \in \mathbb{R}$  to a sequence of  $D$  elements (i.e.,  $D$  numerals in a balanced number system) in  $\{(x_{D-1}, \dots, x_1, x_0) | x_i \in \mathbb{S}_\beta, \beta > 1, i \in \mathbb{Z}_D\}$  as

$$(x_{D-1}, \dots, x_1, x_0) = f_{\text{enc},\beta}(v), \quad (7)$$

where  $\beta$  is an odd positive integer (called base or scale [42]),  $x_i$  is referred to as a numeral at the  $i$ th position, and  $\mathbb{S}_\beta$  is the

symbol set. Without loss of generality, we define the symbol set  $\mathbb{S}_\beta$  as

$$\mathbb{S}_\beta \triangleq \{a_j | a_j = f_{\text{bal}}(j), j \in \mathbb{Z}_\beta\}, \quad (8)$$

where  $f_{\text{bal}}(j)$  is defined by

$$f_{\text{bal}}(j) \triangleq \begin{cases} -(j+1)/2, & \text{odd } j, j < \beta - 1 \\ (j+2)/2, & \text{even } j, j < \beta - 1 \\ 0, & j = \beta - 1 \end{cases}. \quad (9)$$

Based on (9),  $a_{\beta-1}$  is a zero-valued symbol. The example symbol sets for  $\beta = 5$  and  $\beta = 7$  can be obtained as  $\mathbb{S}_5 = \{-1, 1, -2, 2, 0\}$  and  $\mathbb{S}_7 = \{-1, 1, -2, 2, -3, 3, 0\}$ , respectively. For a balanced number system, there is no dedicated symbol for sign as  $\mathbb{S}_\beta$  contains negative-valued symbols.

The numerals are obtained via  $f_{\text{enc},\beta}(v)$  as follows: The encoder  $f_{\text{enc},\beta}(v)$  first clamps  $v$  for  $v' = \max(-v_{\text{max}}, \min(v, v_{\text{max}}))$  to ensure  $v' \in [-v_{\text{max}}, v_{\text{max}}]$ . It then re-scales  $v'$  as  $\frac{\xi}{v_{\text{max}}} v' + \xi + \frac{1}{2}$  and maps the scaled value to an integer between 0 and  $2\xi$  with a floor operation for  $\xi \triangleq (\beta^D - 1)/2$ . Afterwards, it expands the corresponding integer as

$$\left\lfloor \frac{\xi}{v_{\text{max}}} v' + \xi + \frac{1}{2} \right\rfloor = \sum_{i=0}^{D-1} b_i \beta^i, \quad (10)$$

for  $b_i \in \mathbb{Z}_\beta$ , where  $(b_{D-1}, \dots, b_0)$  is the (unbalanced) base- $\beta$  representation of the integer. Finally, it calculates the numeral  $x_i$  as  $x_i = b_i - (\beta - 1)/2 \in \mathbb{S}_\beta, \forall i$ .

**Example 1.** Assume that  $\beta = 5$ ,  $D = 3$ , and  $v_{\text{max}} = 1$  and we want to calculate  $f_{\text{enc},\beta}(0.28)$  and  $f_{\text{enc},\beta}(-0.86)$ . By the definition,  $\xi = (5^3 - 1)/2 = 62$ . The base 5 representations of the decimal  $[62 \times 0.28 + 62 + 1/2] = 79$  and the decimal  $[62 \times -0.86 + 62 + 1/2] = 9$  are  $(b_2 b_1 b_0)_5 = (304)_5$  and  $(b_2 b_1 b_0)_5 = (014)_5$ , respectively. Since  $x_i \triangleq b_i - (\beta - 1)/2$ , we obtain  $f_{\text{enc},\beta}(0.28) = (1, -2, 2)$ , and  $f_{\text{enc},\beta}(-0.86) = (-2, -1, 2)$ .

The corresponding decoder  $f_{\text{dec},\beta}$  that maps the sequence  $(x_{D-1}, \dots, x_1, x_0)$  to  $\bar{v} \in \mathbb{R}$  can be expressed as

$$\bar{v} = f_{\text{dec},\beta}(x_{D-1}, \dots, x_1, x_0) \triangleq \frac{v_{\text{max}}}{\xi} \sum_{i=0}^{D-1} x_i \beta^i. \quad (11)$$

**Example 2.** Consider the parameters given in Example 1. Hence, we obtain  $f_{\text{dec},\beta} f_{\text{enc},\beta}(0.28) = f_{\text{dec},\beta}(1, -2, 2) \approx 0.2742$ , and  $f_{\text{dec},\beta} f_{\text{enc},\beta}(-0.86) = f_{\text{dec},\beta}(-2, -1, 2) \approx -0.8548$  based on (11). The step size can also be calculated as  $\Delta = 2/(\beta^3 - 1) \approx 0.016$ .

Note that  $\bar{v} = f_{\text{dec},\beta} f_{\text{enc},\beta}(v)$  forms a mid-tread uniform quantization, i.e., zero is one of the re-construction levels. The quantization step size can also be calculated as  $\Delta = 2v_{\text{max}}/(\beta^D - 1)$  and the quantization error, i.e.,  $|v - \bar{v}|$ , decreases with increasing  $D$  for  $|v| \leq v'_{\text{max}}$  for  $v'_{\text{max}} = v_{\text{max}} + \Delta/2$ .

The operations in  $f_{\text{enc},\beta}$  and  $f_{\text{dec},\beta}$  and the corresponding input-output relationships are given for an arbitrary input in Fig. 1. We utilize  $f_{\text{enc},\beta}$  and  $f_{\text{dec},\beta}$  to encode the local stochastic gradients at the EDs and obtain an estimate of the arithmetic mean of the local stochastic gradients at the ES, respectively, as discussed in Section III.

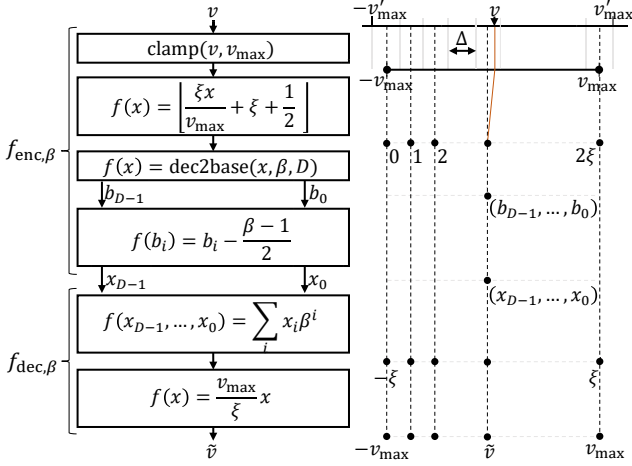


Fig. 1. The operations in  $f_{\text{enc},\beta}$  and  $f_{\text{dec},\beta}$  and the corresponding input-output relationships.

### III. PROPOSED OAC SCHEME

In this section, we discuss the proposed OAC scheme relying on the representation of the gradients based on a balanced number system. We analyze its performance in terms of MSE and introduce the AAM to improve the MSE over the communication rounds of FEEL.

#### A. Key Observation

Based on the discussions given in Section II-B, consider the  $q$ th gradient at the  $k$ th ED for the  $\ell$ th communication round of the FEEL, i.e.,  $\tilde{g}_{k,q}^{(\ell)}$ . Suppose that  $\tilde{g}_{k,q}^{(\ell)}$  is encoded into the sequence of length  $D$  denoted by

$$\left(d_{k,q,D-1}^{(\ell)}, \dots, d_{k,q,1}^{(\ell)}, d_{k,q,0}^{(\ell)}\right) = f_{\text{enc},\beta}(\tilde{g}_{k,q}^{(\ell)}), \quad (12)$$

for  $d_{k,q,i}^{(\ell)} \in \mathbb{S}_\beta$ . By using the definition of  $f_{\text{dec},\beta}$  in (11), the  $q$ th average stochastic gradient, i.e.,  $v_q^{(\ell)} = \frac{1}{K} \sum_{k=0}^{K-1} \tilde{g}_{k,q}^{(\ell)}$ , can be obtained approximately as

$$\begin{aligned} v_q^{(\ell)} &\approx \bar{v}_q^{(\ell)} \triangleq \frac{1}{K} \sum_{k=0}^{K-1} \tilde{g}_{k,q}^{(\ell)} = \frac{v_{\max}}{\xi} \sum_{i=0}^{D-1} \frac{1}{K} \underbrace{\sum_{k=0}^{K-1} d_{k,q,i}^{(\ell)}}_{\triangleq \mu_{q,i}^{(\ell)}} \beta^i \\ &= f_{\text{dec},\beta}(\mu_{q,D-1}^{(\ell)}, \dots, \mu_{q,1}^{(\ell)}, \mu_{q,0}^{(\ell)}), \end{aligned} \quad (13)$$

where  $\bar{g}_{k,q}^{(\ell)}$  is the quantized gradient, i.e.,  $\bar{g}_{k,q}^{(\ell)} = f_{\text{dec},\beta} f_{\text{enc},\beta}(\tilde{g}_{k,q}^{(\ell)})$ .

Equation (13) implies that  $v_q^{(\ell)}$  can be calculated approximately by evaluating the function  $f_{\text{dec},\beta}$  with the values that are calculated by averaging the numerals across  $K$  EDs in the real field, i.e.,  $\{\mu_{q,i}^{(\ell)} | i \in \mathbb{Z}_D\}$ . By evaluating  $\mu_{q,i}^{(\ell)}$  further, it can also be shown that

$$\mu_{q,i}^{(\ell)} = \frac{1}{K} \sum_{k=0}^{K-1} d_{k,q,i}^{(\ell)} = \frac{1}{K} \sum_{j=0}^{\beta-1} a_j K_{q,i,j}, \quad (14)$$

where  $K_{q,i,j}$  denotes the number of EDs with the symbol  $a_j$  for the  $i$ th numeral in (12) and the  $q$ th gradient. Note that

the identity in (14) is due to the definition of expectation for discrete outcomes as given for a probability mass function.

**Example 3.** Assume that  $K = 2$ ,  $\tilde{g}_{0,q}^{(\ell)} = 0.28$ , and  $\tilde{g}_{1,q}^{(\ell)} = -0.86$ . The average of the gradients can be calculated as  $v_q^{(\ell)} = (\tilde{g}_{0,q}^{(\ell)} + \tilde{g}_{1,q}^{(\ell)})/2 = -0.29$ . Now, consider the encoder parameters given in Example 1. We obtain  $f_{\text{enc},\beta}(0.28) = (1, -2, 2)$ , and  $f_{\text{enc},\beta}(-0.86) = (-2, -1, 2)$ . Therefore, the average of the numerals can be calculated as  $(\mu_{q,2}^{(\ell)}, \mu_{q,1}^{(\ell)}, \mu_{q,0}^{(\ell)}) = (1 - 2, -2 - 1, 2 + 2)/2 = (-1/2, -3/2, 2)$ . Also, notice that  $(\mu_{q,2}^{(\ell)}, \mu_{q,1}^{(\ell)}, \mu_{q,0}^{(\ell)})$  can be calculated by using the number of EDs that votes for each element of  $\{-1, 1, -2, 2, 0\}$ . For instance,  $\mu_{q,0}^{(\ell)}$  can be calculated via the last expression in (14) for  $(K_{q,i,0}, K_{q,i,1}, K_{q,i,2}, K_{q,i,3}, K_{q,i,4}) = (0, 0, 0, 2, 0)$  where the corresponding symbols are  $(a_0, a_1, a_2, a_3, a_4) = (-1, 1, -2, 2, 0)$  for  $\beta = 5$ . By evaluating  $\bar{v}_q^{(\ell)} = f_{\text{dec},\beta}(-1/2, -3/2, 2)$ , we obtain  $\bar{v}_q^{(\ell)} \approx -0.2903$ . Note  $\bar{v}_q^{(\ell)}$  is also equal to the average of the quantized gradients, i.e.,  $f_{\text{dec},\beta} f_{\text{enc},\beta}(0.28) \approx 0.2742$  and  $f_{\text{dec},\beta} f_{\text{enc},\beta}(-0.86) \approx -0.8548$ , as exemplified in Example 2.

The proposed OAC scheme computes an estimate of  $v_q^{(\ell)}$  by relying on the expansion in (13) and the identity given in (14), rather than averaging the continuous  $\tilde{g}_{k,q}^{(\ell)}$  with an analog OAC such as BAA proposed in [10] or Goldenbaum's scheme in [20].

#### B. Edge Device - Transmitter

At the  $\ell$ th communication round of the FEEL, the  $k$ th ED calculates the numerals  $\{d_{k,q,i}^{(\ell)} | q \in \mathbb{Z}_Q, i \in \mathbb{Z}_D\}$  with (12), for a given  $\beta$ . The main strategy exploited at the  $k$ th ED with the proposed scheme is that  $\beta - 1$  subcarriers are dedicated for each numeral and one of them is activated based on its value. To express this encoding operation rigorously, let  $\mathcal{M}$  be a function that maps  $q \in \mathbb{Z}_Q$  to a set of  $(\beta - 1)D$  distinct time-frequency index pairs denoted by  $\mathbb{T}_q \triangleq \{(m_{i,\ell}, l_{i,\ell}) | i \in \mathbb{Z}_D, \ell \in \mathbb{Z}_{\beta-1}\}$  for  $m_{i,\ell} \in \mathbb{Z}_S$  and  $l_{i,\ell} \in \mathbb{Z}_M$ , where  $\mathbb{T}_{q_1} \cap \mathbb{T}_{q_2} = \emptyset$  if  $q_1 \neq q_2$  for  $q_1, q_2 \in \mathbb{Z}_Q$ . The  $k$ th ED determines the modulation symbol  $t_{k,m_{i,\ell},l_{i,\ell}}^{(\ell)}$  as

$$t_{k,m_{i,\ell},l_{i,\ell}}^{(\ell)} = \sqrt{E_s} s_{k,q,i}^{(\ell)} \times \mathbb{I}[d_{k,q,i}^{(\ell)} = a_\ell], \quad (15)$$

for all  $i \in \mathbb{Z}_D$  and  $\ell \in \mathbb{Z}_{\beta-1}$ , where  $E_s$  is a factor to normalize the OFDM symbol energy and  $s_{k,q,i}^{(\ell)}$  is a randomization symbol on the unit circle for peak-to-mean envelope power ratio (PMEPR) reduction [31]. Note that we do not allocate a subcarrier for  $a_{\beta-1} = 0$  as it does not contribute to the sum given in (14). Since we active only one of the  $\beta - 1$  subcarriers in our scheme, we set  $E_s$  to  $\beta - 1$ . After the calculation of (15) for all gradients, the  $k$ th ED calculates the OFDM symbols and all EDs transmit them simultaneously based on the discussions in Section II. Since the proposed scheme uses  $(\beta - 1)D$  subcarriers for each gradient, the maximum number of gradients that can be transmitted on each OFDM symbol can be calculated as  $M_{\text{par}} = \lfloor M / ((\beta - 1)D) \rfloor$  for all EDs.

It is worth emphasizing that the function  $\mathcal{M}$  can be designed based on a scrambler to randomize the synthesized OFDM symbols or an encryption function to enhance the security

of the OAC. We leave these extensions for future work and assume that the function  $\mathcal{M}$  uses  $(\beta-1)D$  adjacent subcarriers for each gradient, as illustrated in Fig. 2. In addition, we do not use TCI to compensate for the multipath channel as this is beneficial to eliminate 1) the need for precise time synchronization, 2) the channel estimation overhead, 3) the information loss due to the truncation, and 4) the instantaneous power fluctuations in fading channel due to the channel inversion. Our scheme also relies on a non-coherent receiver as discussed in Section III-C.

**Example 4.** Consider the parameters given in Example 3, i.e.,  $K = 2$ ,  $\tilde{g}_{0,q}^{(\ell)} = 0.28$ , and  $\tilde{g}_{1,q}^{(\ell)} = -0.86$ , where the local gradients are represented as  $f_{\text{enc},\beta}(0.28) = (d_{0,q,2}^{(\ell)}, d_{0,q,1}^{(\ell)}, d_{0,q,0}^{(\ell)}) = (1, -2, 2)$  for the 0th ED, and  $f_{\text{enc},\beta}(-0.86) = (d_{1,q,2}^{(\ell)}, d_{1,q,1}^{(\ell)}, d_{1,q,0}^{(\ell)}) = (-2, -1, 2)$  for the 1st ED for  $\beta = 5$  and  $D = 3$ . Assume that the resource set for the  $q$ th gradient, i.e.,  $\mathbb{T}_q$ , is given by

$$\begin{aligned} \mathbb{T}_q &= \{(m_{0,0}, l_{0,0}), (m_{0,1}, l_{0,1}), (m_{0,2}, l_{0,2}), (m_{0,3}, l_{0,3}), \\ &\quad (m_{1,0}, l_{1,0}), (m_{1,1}, l_{1,1}), (m_{1,2}, l_{1,2}), (m_{1,3}, l_{1,3}), \\ &\quad (m_{2,0}, l_{2,0}), (m_{2,1}, l_{2,1}), (m_{2,2}, l_{2,2}), (m_{2,3}, l_{2,3}), \} \\ &= \{(0, 0), (0, 1), \dots, (0, 11)\}, \end{aligned}$$

i.e., the first 12 adjacent subcarriers of the 0th OFDM symbol. Based on (8),  $\mathbb{S}_5 = \{a_0 = -1, a_1 = 1, a_2 = -2, a_3 = 2, a_4 = 0\}$ . Hence, based on (15), the activated subcarriers for the 0th ED (with omitting the randomization symbols for readability) are given by

$$(t_{0,0,0}^{(\ell)}, \dots, t_{0,0,11}^{(\ell)}) = (\underbrace{0, 0, 0, \sqrt{E_s}, 0, 0, \sqrt{E_s}, 0, 0, \sqrt{E_s}, 0, 0}_{i=0}, \underbrace{0, 0, 0, \sqrt{E_s}, 0, 0, \sqrt{E_s}, 0, 0, \sqrt{E_s}, 0, 0}_{i=1}, \underbrace{0, 0, 0, \sqrt{E_s}, 0, 0, \sqrt{E_s}, 0, 0, \sqrt{E_s}, 0, 0}_{i=2}),$$

as  $\mathbb{I}[d_{0,q,i}^{(\ell)} = a_\ell] = 1$  for  $(i = 0, \ell = 3)$ ,  $(i = 1, \ell = 2)$ , and  $(i = 2, \ell = 1)$ . For the first ED, the active subcarriers are given by

$$(t_{1,0,0}^{(\ell)}, \dots, t_{1,0,11}^{(\ell)}) = (\underbrace{0, 0, 0, \sqrt{E_s}, \sqrt{E_s}, 0, 0, 0, 0, 0, \sqrt{E_s}, 0}_{i=0}, \underbrace{0, 0, 0, \sqrt{E_s}, \sqrt{E_s}, 0, 0, 0, 0, 0, \sqrt{E_s}, 0}_{i=1}, \underbrace{0, 0, 0, \sqrt{E_s}, \sqrt{E_s}, 0, 0, 0, 0, 0, \sqrt{E_s}, 0}_{i=2}).$$

as  $\mathbb{I}[d_{0,q,i}^{(\ell)} = a_\ell] = 1$  for  $(i = 0, \ell = 0)$ ,  $(i = 1, \ell = 2)$ , and  $(i = 2, \ell = 2)$ .

**Remark 1.** For  $D = 1$ , the proposed scheme divides  $[-v_{\text{max}}, v_{\text{max}}]$  into  $\beta - 1$  equal intervals (or equivalently  $[-v'_{\text{max}}, v'_{\text{max}}]$  into  $\beta$  intervals) and the modulation is  $(\beta - 1)$ -ary FSK over OFDM, i.e., the scheme encodes the amplitude information into a subcarrier index via  $f_{\text{enc},\beta}$ .

### C. Edge Server - Receiver

At the ES, we assume that the CSI, i.e.,  $\{\mathbf{h}_{k,m,l}^{(\ell)} | k \in \mathbb{Z}_K, l \in \mathbb{Z}_M, m \in \mathbb{Z}_S\}$ , is *not* available. Hence, the ES exploits that  $\mathbf{r}_{m_i,\ell,l_i,\ell}^{(\ell)}$  is a random vector for  $\mathbf{r}_{m_i,\ell,l_i,\ell}^{(\ell)} \sim \mathcal{CN}(\mathbf{0}_R, (E_s K_{q,i,\ell} + \sigma_n^2) \mathbf{I}_R)$  and obtains an estimate of  $\{\hat{K}_{q,i,\ell} | \ell \in \mathbb{Z}_{\beta-1}\}$ , non-coherently. For given  $i$  and  $q$ , by

using the corresponding log-likelihood function, the maximum likelihood (ML) detector can be expressed as

$$\begin{aligned} \{\hat{K}_{q,i,\ell} | \ell \in \mathbb{Z}_{\beta-1}\} &= \arg \min_{\{K_\ell\}} \left\{ \sum_{\ell=0}^{\beta-2} \ln \det \boldsymbol{\Sigma}_\ell + \mathbf{x}_\ell^H \boldsymbol{\Sigma}_\ell^{-1} \mathbf{x}_\ell \right\} \\ &\text{s.t. } \sum_{\ell=0}^{\beta-2} K_\ell \leq K, K_\ell \in \{0, \dots, K\}, \forall \ell \end{aligned} \quad (16)$$

where  $\mathbf{x}_\ell = [\Re\{\mathbf{r}_{m_i,\ell,l_i,\ell}^{(\ell)}\}^T \Im\{\mathbf{r}_{m_i,\ell,l_i,\ell}^{(\ell)}\}^T]^T$  and  $\boldsymbol{\Sigma}_\ell = \frac{E_s K_\ell + \sigma_n^2}{2} \mathbf{I}_{2R}$ . However, due to the constraints, a solution to (16) can increase the receiver complexity considerably. To address this issue, we relax the constraints and evaluate  $\hat{K}_{q,i,\ell}$  independently as given by

$$\begin{aligned} \hat{K}_{q,i,\ell} &= \arg \min_{K_\ell} \left\{ 2R \ln \left( \frac{E_s K_\ell + \sigma_n^2}{2} \right) + \frac{2 \|\mathbf{r}_{m_i,\ell,l_i,\ell}^{(\ell)}\|_2^2}{E_s K_\ell + \sigma_n^2} \right\} \\ &= \frac{\|\mathbf{r}_{m_i,\ell,l_i,\ell}^{(\ell)}\|_2^2}{E_s R} - \frac{\sigma_n^2}{E_s}. \end{aligned} \quad (17)$$

Therefore, a low-complexity estimator of  $\mu_{q,i}^{(\ell)}$  can be obtained as

$$\hat{\mu}_{q,i}^{(\ell)} = \frac{1}{K} \sum_{\ell=0}^{\beta-2} a_\ell \hat{K}_{q,i,\ell}. \quad (18)$$

Finally, the estimator of  $v_q^{(\ell)}$  can be expressed as

$$\hat{v}_q^{(\ell)} = f_{\text{dec},\beta} \left( \hat{\mu}_{q,D-1}^{(\ell)}, \dots, \hat{\mu}_{q,1}^{(\ell)}, \hat{\mu}_{q,0}^{(\ell)} \right). \quad (19)$$

The ES finally transmits  $\hat{\mathbf{v}}^{(\ell)}$  to the EDs for the next communication round and the  $k$ th ED updates its parameters as  $\mathbf{w}^{(\ell+1)} = \mathbf{w}^{(\ell)} - \eta \hat{\mathbf{v}}^{(\ell)}$ ,  $\forall k$ . The corresponding transmitter and receiver diagrams are provided in Fig. 2.

### D. MSE Analysis

For a given set of local stochastic gradients (i.e., given  $K_{q,i,\ell}$ ),  $\mathbf{r}_{m_i,\ell,l_i,\ell}^{(\ell)} \sim \mathcal{CN}(\mathbf{0}_R, (E_s K_{q,i,\ell} + \sigma_n^2) \mathbf{I}_R)$  holds for Rayleigh fading channel. Since the absolute square of an element of  $\mathbf{r}_{m_i,\ell,l_i,\ell}^{(\ell)}$  is an exponential distribution with the mean  $E_s K_{q,i,\ell} + \sigma_n^2$ , the distribution of  $\|\mathbf{r}_{m_i,\ell,l_i,\ell}^{(\ell)}\|_2^2 / R$  can be obtained as  $\Gamma(R, R / (E_s K_{q,i,\ell} + \sigma_n^2))$ . As a result, the mean and the variance of the estimator  $\hat{K}_{q,i,\ell}$  can be calculated through the properties of a gamma distribution as

$$\mathbb{E}[\hat{K}_{q,i,\ell}] = \frac{\mathbb{E}[\|\mathbf{r}_{m_i,\ell,l_i,\ell}^{(\ell)}\|_2^2 / R]}{E_s} - \frac{\sigma_n^2}{E_s} = K_{q,i,\ell}, \quad (20)$$

and

$$\text{var}(\hat{K}_{q,i,\ell}) = \frac{\text{var}(\|\mathbf{r}_{m_i,\ell,l_i,\ell}^{(\ell)}\|_2^2 / R)}{E_s} = \frac{1}{R} \left( K_{q,i,\ell} + \frac{\sigma_n^2}{E_s} \right)^2, \quad (21)$$

respectively, where the expectation is calculated over the randomness of the channel and noise. Hence,  $\hat{K}_{q,i,\ell}$  is an unbiased estimator. Also, based on (18) and (19), both  $\hat{\mu}_{q,i}^{(\ell)}$

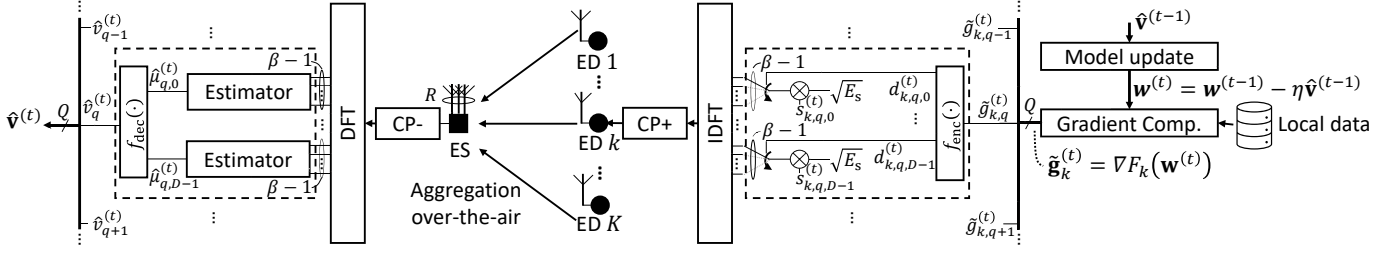


Fig. 2. The transmitter and received diagrams with the proposed OAC scheme for FEEL.

and  $\hat{v}_q^{(\ell)}$  are unbiased estimators of  $\mu_{q,i}^{(\ell)}$  and  $\bar{v}_q^{(\ell)}$ , respectively. For a given  $\{K_{q,i,\ell} | \ell \in \mathbb{Z}_{\beta-1}\}$ , by using (18) and (21), the variance of the estimator  $\hat{\mu}_{q,i}^{(\ell)}$  is obtained as

$$\text{var}(\hat{\mu}_{q,i}^{(\ell)}) = \frac{1}{RK^2} \sum_{\ell=0}^{\beta-2} a_{\ell}^2 \left( K_{q,i,\ell} + \frac{\sigma_n^2}{E_s} \right)^2. \quad (22)$$

Therefore, we can calculate the variance of the estimator  $\hat{v}_q^{(\ell)}$  as

$$\text{var}(\hat{v}_q^{(\ell)}) = \frac{v_{\max}^2}{\xi^2 RK^2} \sum_{i=0}^{D-1} \sum_{\ell=0}^{\beta-2} a_{\ell}^2 \left( K_{q,i,\ell} + \frac{\sigma_n^2}{E_s} \right)^2 \beta^{2i}. \quad (23)$$

Hence, the (classical) MSE of the estimator  $\hat{v}_q^{(\ell)}$  can be obtained as

$$\text{MSE}(\hat{v}_q^{(\ell)}) = \text{var}(\hat{v}_q^{(\ell)}) + \frac{1}{K^2} \left( \sum_{k=0}^{K-1} \bar{g}_{k,q}^{(\ell)} - \bar{g}_{k,q}^{(\ell)} \right)^2,$$

where the last term is the squared bias, i.e.,  $(v_q^{(\ell)} - \bar{v}_q^{(\ell)})^2$ , due to the quantization.

The BMSE of the estimator  $\hat{v}_q^{(\ell)}$  can be calculated as

$$\begin{aligned} \text{BMSE}(\hat{v}_q^{(\ell)}) &= \mathbb{E} \left[ \text{MSE}(\hat{v}_q^{(\ell)}) \right] \\ &= \underbrace{\mathbb{E}_{\bar{v}_q^{(\ell)}} \left[ \left( \hat{v}_q^{(\ell)} - \bar{v}_q^{(\ell)} \right)^2 \right]}_{\sigma_{\text{channel}}^2} + \underbrace{\mathbb{E}_{\bar{v}_q^{(\ell)}} \left[ \left( \bar{v}_q^{(\ell)} - v_q^{(\ell)} \right)^2 \right]}_{\sigma_{\text{quan}}^2} \end{aligned}$$

To derive the BMSE, we assume that the distribution of  $\bar{g}_{k,q}^{(\ell)}$  is  $\mathcal{U}(-v'_{\max}, v'_{\max})$ . Based on the derivation given in Appendix A,  $\sigma_{\text{channel}}^2$  can be calculated as

$$\sigma_{\text{channel}}^2 = v_{\max}^2 \underbrace{\frac{1}{3R} \left( \frac{1}{\beta} \left( 1 + \frac{\beta \sigma_n^2}{K(\beta-1)} \right)^2 + \frac{\beta}{K(\beta-1)} \right)}_{E_{\text{channel}}} \frac{\beta^D + 1}{\beta^D - 1}. \quad (24)$$

Since  $d_{k,q,i}^{(\ell)}$  follows a uniform distribution for  $\bar{g}_{k,q}^{(\ell)} \sim \mathcal{U}(-v'_{\max}, v'_{\max})$ , we can obtain  $\sigma_{\text{quan}}^2$  as

$$\sigma_{\text{quan}}^2 = v_{\max}^2 \underbrace{\frac{1}{3K(\beta^D - 1)^2}}_{E_{\text{quan}}}. \quad (25)$$

Therefore, the BMSE can be calculated as

$$\text{BMSE}(\hat{v}_q^{(\ell)}) = \sigma_{\text{channel}}^2 + \sigma_{\text{quan}}^2 = v_{\max}^2 E_{\text{total}}, \quad (26)$$

where  $E_{\text{total}}$  is  $E_{\text{channel}} + E_{\text{quan}}$ .

In practice, the gradients often have an unknown probability distribution that changes over the communication rounds [14]. Hence, the expression in (26) has limitations due to the underlying distribution assumption. On the other hand, the analysis with a general non-stationary distribution is much more complicated because the expected value in (31) for different numerals may not be identical to each other. Nevertheless, (26) is a closed-form expression and predicts the performance of the scheme for a given configuration roughly without using sophisticated expressions, as exemplified in Section V.

Based on (26), we infer the followings: 1) The BMSE decreases with increasing  $\beta$  as both  $E_{\text{channel}}$  and  $E_{\text{quan}}$  tend to be smaller with a larger  $\beta$ . While increasing the number of numerals  $D$  decreases the factor  $E_{\text{quan}}$ , its impact on the factor  $E_{\text{channel}}$  is limited as the limit of  $\beta^D + 1/(\beta^D - 1)$  is 1 as  $D$  approaches infinity. 2) BMSE decreases with the number of antennas in cases where the impact of the quantization error on the error is small for a larger  $\beta$  or a larger  $D$ . 3) The impact of the quantization error on the BMSE rapidly diminishes either by increasing  $\beta$  or  $D$ . 4) The impact of  $\sigma_n^2$  on the BMSE decreases with the increasing number of EDs. 5) With increasing  $K$  or  $\beta^D$ , the BMSE asymptotically decreases to  $v_{\max}^2/(3R\beta)$ .

As we show in Section IV and demonstrate in Section V, quantization error plays a major role in the convergence rate of the FEEL. To reduce quantization error over the communication rounds of FEEL, we introduce a simple method in the following subsection.

#### E. Adaptive Absolute Maximum (AAM)

Without any adaptation, the BMSE in (26) is a constant, and the error due to the proposed scheme can dominate the estimate of  $v_q^{(\ell)}$  when its value is closer to 0. This can be a non-negligible issue in practice because the gradients tend to become smaller over time. To address this issue, we exploit the fact that the gradients between adjacent communication rounds may have a high correlation [38] and propose to improve the proposed scheme with a feedback loop where all the EDs transmit only a *single* parameter related to their local gradients to the ES through a control channel (e.g., PUCCH in 3GPP 5G NR) and the ES sets up a new absolute maximum  $v_{\max}$  for

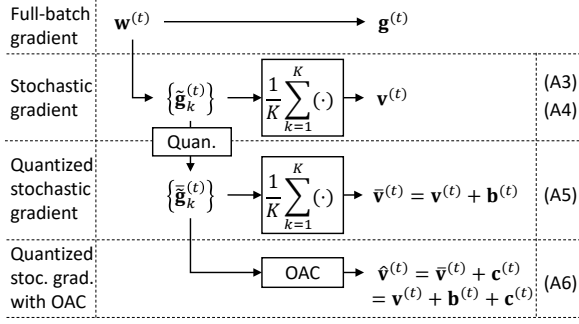


Fig. 3. Relationships between the variables and the assumptions. Assumptions 3-6 are denoted as A3-A6, respectively.

the next communication round based on the received feedback from the EDs. The information that is transmitted from ED can be a function of the maximum absolute value of the gradients, the empirical variance, the standard deviation, or the mean of the gradients. In this study, we assume that the feedback loop realizes the AAM as

$$v_{\max}^{(\ell)} = \alpha \times \|\mathbf{m}^{(\ell-1)}\|_{\infty}, \quad (27)$$

where  $\mathbf{m}^{(\ell)} = [m_0^{(\ell)}, \dots, m_{K-1}^{(\ell)}]$  is the metric vector,  $m_k^{(\ell)}$  is the metric for the  $k$ th ED,  $\forall k$ ,  $\alpha$  is a positive value, and  $v_{\max}^{(0)}$  is the initial value for the AAM. The AAM based on (27) can be implemented in a practical network as follows: 1) The  $k$ th ED transmits  $m_k^{(\ell)}$ ,  $\forall k$ , at the  $\ell$ th communication round through an orthogonal channel. 2) The ES calculates (27). 3) The ES transmits  $v_{\max}^{(\ell+1)}$  to the EDs. 4) The EDs update  $f_{\text{enc},\beta}$  with the new absolute maximum  $v_{\max}^{(\ell+1)}$ .

In this study, we choose  $m_k^{(\ell)} = \|\tilde{\mathbf{g}}_k^{(\ell)}\|_2$  and  $\alpha = 5/\sqrt{Q}$ , heuristically, based on five-sigma deviation rule. The convergence rate of FEEL with and without AAM is analyzed in Section IV.

#### IV. CONVERGENCE ANALYSIS

For the convergence rate analysis, we consider well-known Lipschitz continuity [43] and make several assumptions on the loss function and gradient estimates, given as follows:

**Definition 1.** A function  $f$  is  $L$ -Lipschitz over a set  $S$  with respect to a norm  $\|\cdot\|$  if there exists a real constant  $L > 0$  such that  $\|f(\mathbf{y}) - f(\mathbf{x})\| \leq L\|\mathbf{y} - \mathbf{x}\|$ ,  $\forall \mathbf{x}, \mathbf{y} \in S$ .

**Lemma 1** ([43, Lemma 1.2.3]). For a differentiable function  $f: \mathbb{R}^Q \rightarrow \mathbb{R}$ , let  $\nabla f$  be  $L$ -Lipschitz on  $\mathbb{R}^Q$  with respect to norm  $\|\cdot\|_2$ . Then, for any  $\mathbf{y}, \mathbf{x}$  from  $\mathbb{R}^Q$ ,

$$|f(\mathbf{y}) - f(\mathbf{x}) - \nabla f(\mathbf{x})^T(\mathbf{y} - \mathbf{x})| \leq \frac{L}{2} \|\mathbf{y} - \mathbf{x}\|_2^2. \quad (28)$$

**Assumption 1** (Bounded loss function). The loss function is bounded, i.e.,  $F(\mathbf{w}) \geq F^*$ ,  $\forall \mathbf{w}$ .

**Assumption 2** (Smooth gradients). The gradient of the loss function, i.e.,  $\nabla F$ , is  $L$ -Lipschitz on  $\mathbb{R}^Q$  with respect to the norm  $\|\cdot\|_2$ , i.e.,  $\|\nabla F(\mathbf{w}') - \nabla F(\mathbf{w})\|_2 \leq L\|\mathbf{w}' - \mathbf{w}\|_2$ ,  $\forall \mathbf{w}, \mathbf{w}' \in \mathbb{R}^Q$ .

Assumption 1 and Assumption 2 are the standard assumptions that are often made in the literature for convergence analysis.

**Assumption 3** (Unbiased average local stochastic gradients). The average stochastic gradient vector is an unbiased estimate of the global gradient vector, i.e.,  $\mathbb{E}[\mathbf{v}^{(\ell)}] = \mathbf{g}^{(\ell)}$ .

**Assumption 4** (Gradient divergence). For all  $\mathbf{w}^{(\ell)}$ , the second-order moments of the local stochastic gradients of the  $k$ th ED with respect to the global gradients is bounded as  $\mathbb{E}[\|\tilde{\mathbf{g}}_k^{(\ell)} - \mathbf{g}^{(\ell)}\|_2^2] \leq \delta_k$ ,  $\forall k$ . This assumption implies that  $\mathbb{E}[\|\mathbf{v}^{(\ell)} - \mathbf{g}^{(\ell)}\|_2^2] \leq \frac{1}{K} \sum_{k=0}^{K-1} \delta_k$ .

Assumption 3 and Assumption 4 do not require the local gradients to be unbiased estimates of the global gradients. Hence, they are compatible with a heterogeneous data distribution scenario where the *sum* of local gradients is unbiased.

**Assumption 5** (Average quantization bias). Let  $\mathbf{b}^{(\ell)} \triangleq \bar{\mathbf{v}}^{(\ell)} - \mathbf{v}^{(\ell)} = \frac{1}{K} \sum_{k=1}^K \tilde{\tilde{\mathbf{g}}}_k^{(\ell)} - \tilde{\mathbf{g}}_k^{(\ell)}$  be the quantization bias averaged across the EDs. The expected value of the average quantization bias is zero, i.e.,  $\mathbb{E}[\mathbf{b}^{(\ell)}] = \mathbf{0}_Q$ .

Assumption 5 gets weaker with increasing  $K$  due to the averaging across the EDs or reducing the quantization step by increasing  $\beta$  or  $D$ .

**Assumption 6** (MSE bound). Let us express the aggregated gradient with OAC as  $\hat{\mathbf{v}}^{(\ell)} = \mathbf{v}^{(\ell)} + \mathbf{b}^{(\ell)} + \mathbf{c}^{(\ell)}$ , where  $\mathbf{c}^{(\ell)}$  is the noise due to the OAC. The average MSE due to the communication channel and the quantization is bounded by  $\mathbb{E}[\|\hat{\mathbf{v}}^{(\ell)} - \mathbf{v}^{(\ell)}\|_2^2] \leq Q(\sigma_{\text{channel}}^2 + \sigma_{\text{quan}}^2)$ .

It is worth noting that the expected value of the channel noise is zero, i.e.,  $\mathbb{E}[\mathbf{c}^{(\ell)}] = \mathbf{0}_Q$  since  $\hat{\mathbf{v}}_q^{(\ell)}$  is an unbiased estimator  $\hat{v}_q^{(\ell)}$ . The relationship between the variables and the assumptions are given in Fig. 3 for clarity.

**Theorem 1.** For a fixed learning rate  $\eta$ , the convergence rate of the distributed training based on the proposed scheme in the Rayleigh channel is

$$\mathbb{E} \left[ \frac{1}{T} \sum_{\ell=0}^{T-1} \|\mathbf{g}^{(\ell)}\|_2^2 \right] \leq \frac{1}{T\eta \left(1 - \frac{\eta L}{2}\right)} \left( F(\mathbf{w}^{(0)}) - F^* \right) + \frac{\frac{\eta L}{2}}{1 - \frac{\eta L}{2}} \left( (\sigma_{\text{channel}}^2 + \sigma_{\text{quan}}^2)Q + \frac{1}{K} \sum_{k=0}^{K-1} \delta_k \right), \quad (29)$$

where  $\sigma_{\text{channel}}^2$  and  $\sigma_{\text{quan}}^2$  are given in (24) and (25), respectively.

The proof is given in Appendix B.

Theorem 1 is an extension of the convergence analysis of SGD under the consideration of the proposed scheme. While the first term of the bound given in (29) becomes smaller for a larger total number of communication rounds  $T$ , the noise ball is determined with the values of the learning rate  $\eta$ , the noise variance due to the local stochastic gradient estimates, and the noise due to the proposed scheme. The noise ball decreases when a smaller learning rate  $\eta$  is used at the expense of a larger  $T$  due to the first term in (29). The proposed scheme

contributes to the noise variance due to stochastic gradient calculation in (6). Hence, the standard tuning methods for SGD such as momentum can also be utilized with the proposed scheme to improve the convergence rate.

The convergence rate of the FEEL under the presence of the proposed scheme with AAM based on (27) can be expressed as follows:

**Theorem 2.** For a fixed learning rate  $\eta$ , the convergence rate of the distributed training based on the proposed scheme with AAM in the Rayleigh channel is

$$\begin{aligned} \mathbb{E} \left[ \frac{1}{T} \sum_{\ell=1}^T \|\mathbf{g}^{(\ell)}\|_2^2 \right] &\leq \frac{1}{T\eta \left(1 - \frac{\eta L'}{2}\right)} \left( F(\mathbf{w}^{(1)}) - F^* \right. \\ &\quad \left. + \frac{\eta L'}{2} \alpha^2 E_{\text{total}} K \mathbb{E} \left[ \|\mathbf{g}^{(0)}\|_2^2 - \|\mathbf{g}^{(T)}\|_2^2 \right] \right) \\ &\quad + \frac{\frac{\eta L'}{2}}{1 - \frac{\eta L'}{2}} \frac{1}{K} \sum_{k=0}^{K-1} \delta_k, \end{aligned} \quad (30)$$

where  $L' = L(1 + \alpha^2 E_{\text{total}} K)$  for  $K_{q,i,\ell} \sim \mathcal{B}(K, 1/\beta)$  for all  $\ell, i, q$ .

The proof is given in Appendix C.

Theorem (2) shows that the AAM eliminates the additive impact of the proposed scheme on the noise on the gradients (as in Theorem 1) at the expense of scaling up the constant  $L$ . As compared to the case without AAM, the noisy ball is smaller with AAM. Hence, the convergence rate improves considerably, as demonstrated in Section V.

## V. NUMERICAL RESULTS

In this section, we assess the proposed scheme numerically for  $D \in \{1, 2\}$  and  $\beta \in \{3, 5, 7\}$ . We demonstrate its BMSE performance and the test accuracy results based on FEEL under homogeneous and heterogeneous data distributions. For the comparisons, we consider Goldenbaum's scheme (without channel inversion) [20], [34] and FSK-MV [22], [31] since they rely on non-coherent techniques, similar to the proposed scheme. We also provide the results without OAC based on SGD. We do not consider methods based on channel inversion techniques as their performance can deteriorate quickly in the presence of synchronization errors [31], [32].

Goldenbaum's scheme aims to compute continuous-valued functions based on analog modulation. After the symbol at the  $k$ th ED is processed with a function  $\epsilon(x) = ax + b$  that results in a non-negative value for  $a = 1/v_{\max}$  and  $b = v_{\max}$ , the square root of the resulting value is multiplied with a unimodular sequence of length  $L$  as  $\sqrt{\epsilon(\tilde{g}_{k,q}^{(\ell)})} \times [e^{j\theta_{k,1}}, \dots, e^{j\theta_{k,L}}]$ . At the receiver, an estimate of the aggregated symbol is obtained after processing the average energy of the received sequence across  $R$  antennas with another affine function  $\delta(x) = (x - Kb)/a$  to reverse the impact of  $\epsilon(x)$  on the superposed symbols. The main shortcoming of this scheme is that it causes additional interference terms for  $L < K$ . For the numerical analysis, we consider  $L \in \{4, 12\}$  and choose the sequence elements from  $\{1, -1, j, -j\}$  randomly. The EDs transmit the sequences by mapping them to the OFDM subcarriers.

FSK-MV relies on digital modulation to represent two discrete states, i.e.,  $\{-1, 1\}$ , and targets to compute a specific function, i.e., MV, for distributed training by MV. With this method, even if the value of the symbol is very close to 0, the transmitted values are 1 and  $-1$ . Hence, without any precaution, it can bias the training for the scenarios with heterogeneous data distribution.

For all simulations, we consider a single cell with  $K = 25$  EDs. We set the SNR, i.e.,  $1/\sigma_n^2$ , to be 20 dB, and choose the number of antennas at the ES as  $R \in \{1, 25\}$ .

### A. BMSE and error distribution

In this subsection, we analyze the BMSE of the estimator of (19). We calculate the BMSE through simulations for  $\tilde{g}_{k,q}^{(\ell)} \sim \mathcal{U}(-1, 1)$  and  $\tilde{g}_{k,q}^{(\ell)} \sim \mathcal{N}(0, 0.2)$ ,  $\forall k$ . For the proposed scheme, we set  $v_{\max}$  to  $(\beta^D - 1)/\beta^D$  by taking the quantization step into account. For Goldenbaum's scheme, we clamp the outcome if it is not within the range  $[1, 1]$  and set  $v_{\max}$  to 1.

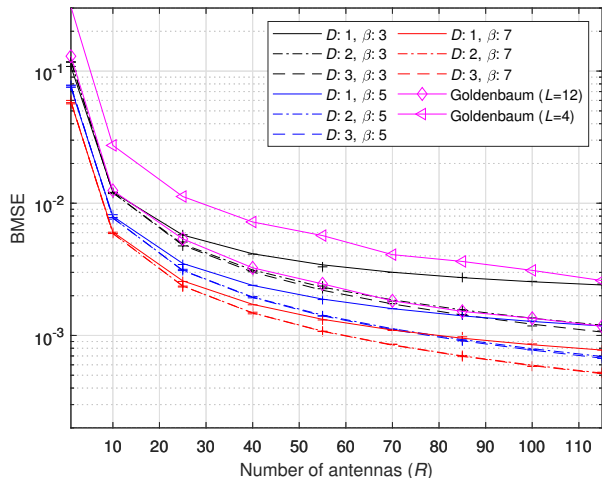
In Fig. 4(a) and Fig. 4(b), we plot the BMSE versus the number of antennas for the uniform and Gaussian distributions, respectively. As can be seen from Fig. 4(a), the simulation results exactly match the theoretical results based on (26). The results are also aligned with the discussions provided in Section III-D. Increasing  $\beta$  reduces the BMSE. While a larger  $D$  decreases the BMSE (by reducing the quantization error), its impact on the BMSE quickly saturates. Similarly, Goldenbaum's scheme performance improves by increasing the number of antennas. However, its performance is slightly worse than the proposed scheme for the same amount of resource consumption. Similar observations can also be made from Fig. 4(b) although the distribution is different from the uniform distribution. We also observe that the theoretical BMSE results are more pessimistic than the ones in this scenario. For example, the BMSE results for the uniform and Gaussian distribution for a single antenna are around 0.1 and 0.07, respectively.

In Fig. 5, we plot the histogram of the error for the uniform distribution. The main observation is that the error distribution for Goldenbaum's scheme is skewed for  $R = 1$  antenna, while it is symmetric for the proposed scheme. For  $R = 25$  antennas, Goldenbaum's scheme becomes less skewed due to the channel hardening.

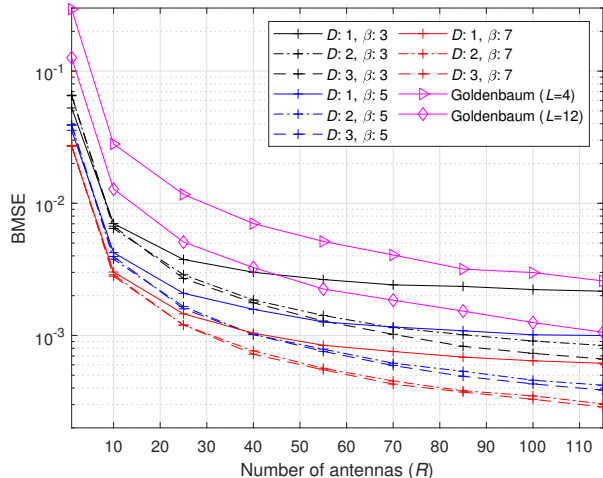
### B. FEEL

To numerically analyze OAC with the proposed scheme for FEEL, we consider the learning task of handwritten-digit recognition. For the fading channel, we consider ITU Extended Pedestrian A (EPA) with no mobility and regenerate the channels between the ES and the EDs independently for each communication round to capture the long-term channel variations. The subcarrier spacing is set to 15 kHz. We use  $M = 1200$  subcarriers (i.e., the signal bandwidth is 18 MHz). Hence, the difference between the time of arrival of the ED signals is maximum  $T_{\text{sync}} = 55.6$  ns. We assume that the synchronization uncertainty at the ES is  $N_{\text{err}} = 3$  samples.

For the local data at the EDs, we use the MNIST database that contains labeled handwritten-digit images size of  $28 \times 28$



(a) Uniform distribution. The curves with the marker '+' and the line '-' are for the simulation and the theoretical results for the proposed method, respectively.



(b) Gaussian distribution (Simulation).

Fig. 4. BMSE versus the number of antennas for  $\tilde{g}_{k,q}^{(\ell)} \sim \mathcal{U}(-1, 1)$  and  $\tilde{g}_{k,q}^{(\ell)} \sim \mathcal{N}(0, 0.2)$ ,  $\forall k (\sigma_n^2 = 0.01, K = 25$  EDs). The proposed scheme provides less error for increasing  $\beta$  and  $D$ .

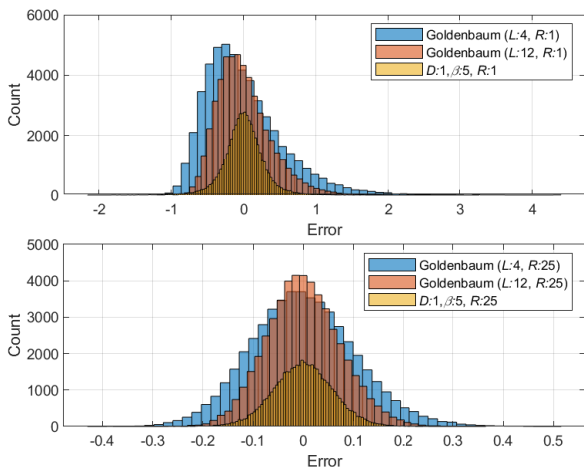


Fig. 5. The error histogram for  $\tilde{g}_{k,q}^{(\ell)} \sim \mathcal{U}(-1, 1)$  ( $\sigma_n^2 = 0.01, K = 25$ , 50000 realizations). While the error distribution for Goldenbaum's scheme is skewed for  $R = 1$  antenna, it is symmetric around 0 for the proposed scheme.

from digit 0 to digit 9. We distribute the data samples in the MNIST database to the EDs to generate representative results for FEEL. We consider both homogeneous and heterogeneous data distributions in the cell. To prepare the data, we first choose  $|\mathcal{D}| = 25000$  training images from the database, where each digit has distinct 2500 images. For the scenario with the homogeneous data distribution, we assume that each ED has 250 distinct images for each digit. As done in [31], for the scenario with the heterogeneous data distribution, we divide the cell into 5 areas with concentric circles and the EDs located in  $u$ th area have the data samples with the labels  $\{u - 1, u, 1 + u, 2 + u, 3 + u, 4 + u\}$  for  $u \in \{1, \dots, 5\}$  (See [31, Figure 3] for an illustration). The number of EDs

in each area is 5. As discussed in Section II, we assume that the path loss is compensated through a power control mechanism. For the model, we consider a convolution neural network (CNN) given in [22, Table I]. At the input layer, standard normalization is applied to the data. Our model has  $Q = 123090$  learnable parameters. For the update rule, the learning rate is set to 0.001. The batch size  $n_b$  is set to 64. To demonstrate the compatibility of the proposed scheme to SGD with momentum, we also provide the test accuracy results when the momentum is 0.9. For the test accuracy calculations, we use 10000 test samples available in the MNIST database.

In Fig. 6, we provide the test accuracy versus communication rounds for the scenario with homogeneous data distribution for  $R = 1$  antenna. In Fig. 6(a), the momentum is zero and we do not consider the AAM and set  $v_{\max} = 1$ . For this scenario, the accuracy results improve with the proposed scheme for larger  $\beta$  or  $D$  (i.e., less  $\sigma_{\text{channel}}^2$ ). The proposed scheme without AAM becomes more blind to the gradients over the communication rounds as their magnitudes tend to reduce. The FSK-MV is superior to the proposed scheme because FSK-MV is based on signSGD, while the proposed scheme implements SGD and the proposed scheme increases the noise on the gradient estimates as predicted by Theorem 1. In [24], it was also mentioned that signSGD can outperform SGD by providing stronger weight to the gradient direction as compared to SGD when the gradients are noisy. Goldenbaum's scheme performs similarly to the proposed scheme for large  $\beta$  and  $D$ . However, since it is based on analog modulation, it is much more robust to quantization errors as compared to the proposed scheme without AAM. In Fig. 6(c), we re-run the simulation with AAM. In this case, the convergence rate improves considerably for all  $\beta$  and  $D$  since AAM eliminates the additive noise term due to the proposed scheme in Theorem 1. The performance with the choice of  $\{\beta = 3, D = 1\}$  is worse than the other configurations

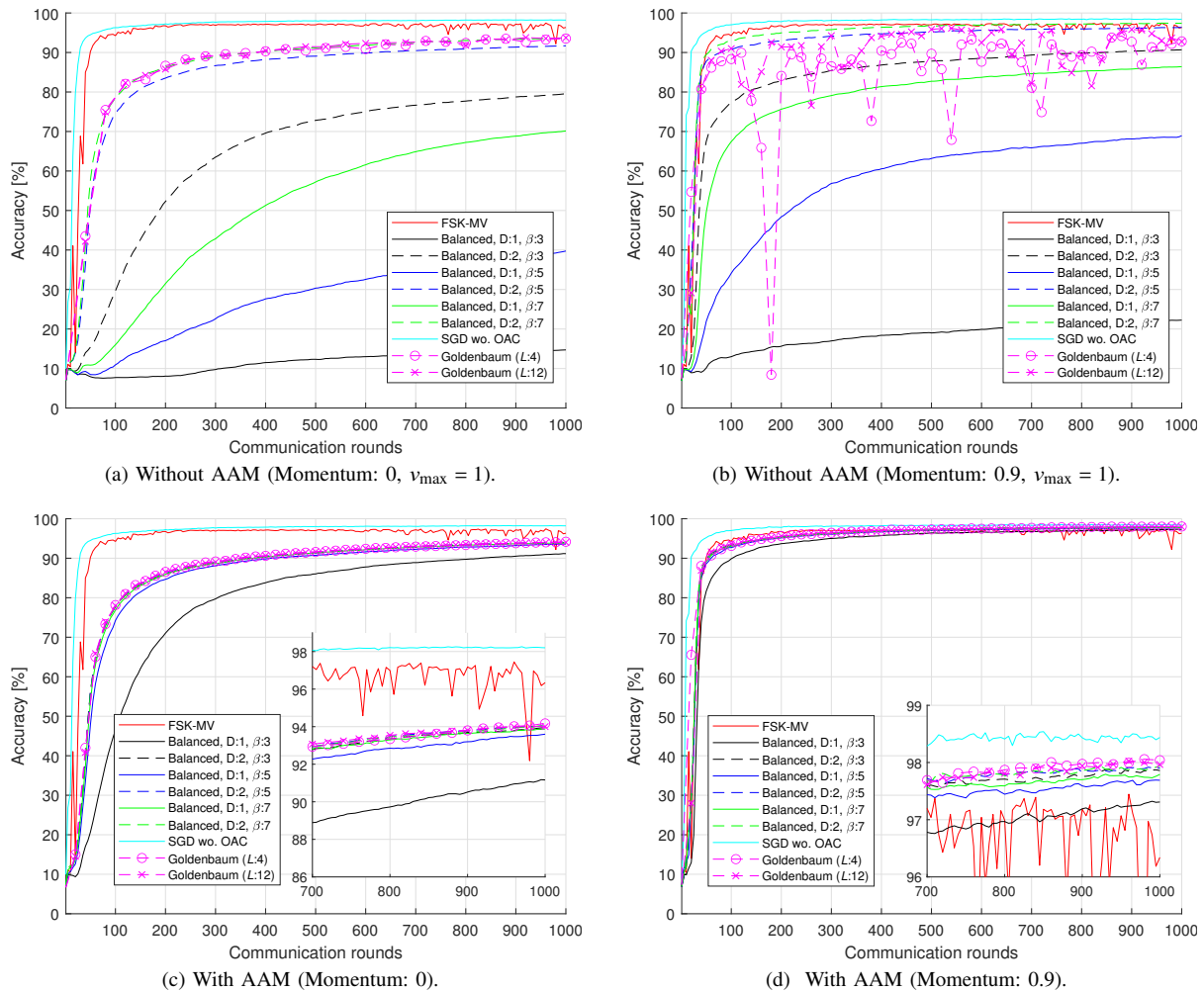


Fig. 6. Test accuracy versus communication rounds (Homogeneous data distribution,  $R = 1$ ,  $K = 25$ ). The proposed scheme with AAM addresses the quantization errors.

since the quantization error is dominant in the case. The best performance is obtained with the FSK-MV due to its inherent benefits of signSGD. In Fig. 6(b), SGD is used with the momentum. A non-zero momentum improves the convergence rates for all configurations. However, it causes an unstable behavior for Goldenbaum's scheme, which may be due to the skewed error distribution shown in Fig. 5. In Fig. 6(d), we re-evaluate the same configurations with the AAM. In this case, both test accuracy and the convergence rate are improved for the proposed scheme. Also, the final test accuracy reaches almost 98%, better than the one with FSK-MV. Similarly, AAM also improves Goldenbaum's scheme while addressing the instability.

In Fig. 7, we consider  $R = 25$  antennas. Although using more antennas can improve the BMSE considerably, its impact on the test accuracy for the proposed scheme is almost negligible. This is because using more antennas reduces the channel noise as in Fig. 4, but it cannot reduce the quantization noise which is a function of  $v_{\max}$  and the gradient distribution changing over communication rounds. The results in Fig. 7 indicate that the proposed scheme can achieve notable test accuracy results if the quantization error is reduced at the

expense of more resource consumption even when there is only a *single* antenna at the ES. As can be seen from Fig. 7(c), the instability of the Goldenbaum's scheme in Fig. 6(c) is addressed with more antennas.

In Fig. 8, the test accuracy is evaluated when the data distribution is highly heterogeneous, i.e., each ED has only 6 unique digits. In this case, the performance of the FSK-MV degrades drastically, whereas the performance of the proposed scheme is similar to the one in Fig. 6. The test accuracy under heterogeneous data distribution is less than 80% for the FSK-MV (this is also reported in [31]). This is because of the bias in the MV for the heterogeneous data distribution scenario. For example, the digits 0 and 9 are available at fewer EDs, which makes the MV biased. Hence, the training does not learn these digits well. On the other hand, the proposed scheme with large  $\beta$  and  $D$  can achieve more than 90% test accuracy as shown in Fig. 8 for  $R = 1$ . A similar observation can be made for  $R = 25$  as in Fig. 9(a)-(d), i.e., the proposed scheme can provide test accuracy up to 98% even if the data distribution is not homogeneous.

In Fig. 10, we provide the simulation results for CIFAR10 ( $|\mathcal{D}| = 50000$ ). For CIFAR10, the neural network in [22,

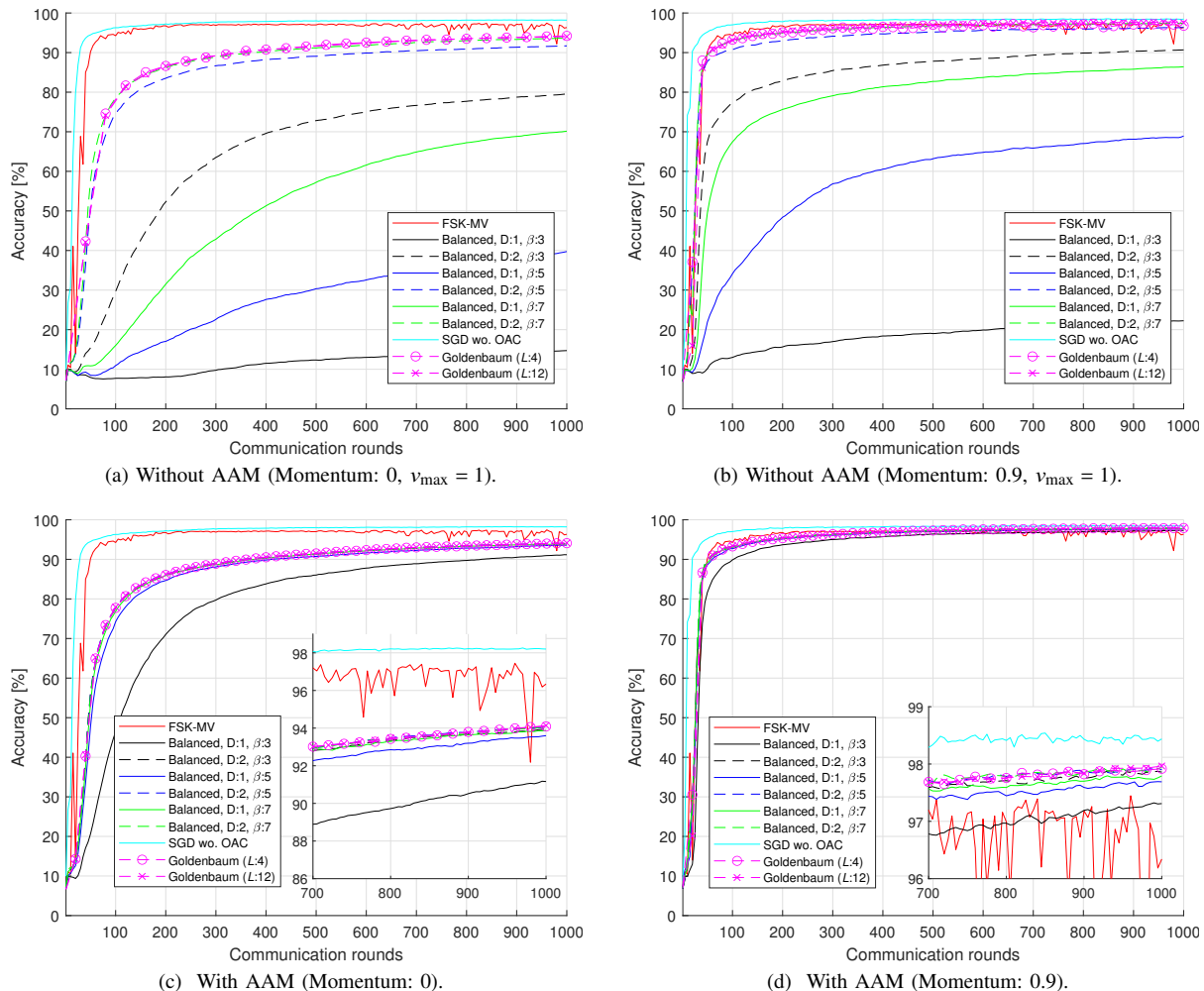


Fig. 7. Test accuracy versus communication rounds (Homogeneous data distribution,  $R = 25$ ,  $K = 25$ ). Increasing the number of antennas has a negligible effect on the test accuracy for the proposed scheme.

Table I] is extended to three channels, where the size of each channel is 32 by 32. It is well-known that CIFAR10 is a more challenging dataset than MNIST and the test accuracy is less than 70 percent. However, the relative orders of the curves for the proposed scheme are consistent with ones in Fig.6(c) and Fig.8(c))

## VI. CONCLUDING REMARKS

In this study, we investigate an OAC method that exploits balanced number systems for gradient aggregation. The proposed scheme achieves a continuous-valued computation through a digital scheme by exploiting the fact that the average of the numerals in the real domain can be used to compute the average of the corresponding real-valued parameters approximately. With the proposed OAC method, the local stochastic gradients are encoded into a sequence where the elements of the sequence determine the activated OFDM subcarriers. We also use a non-coherent receiver to eliminate the precise sample-level time synchronization, channel estimation overhead, and power instabilities due to the channel inversion techniques. To improve its MSE performance, we

also introduce AAM. We theoretically analyze its MSE performance and its convergence rate for FEEL by considering both homogeneous and heterogeneous distributions. Our numerical results demonstrate that the test accuracy of the FEEL with the proposed scheme using AAM can reach up to 98% even when the EDs do not have all labels in their data sets.

The proposed scheme provides a potentially rich area to be investigated. For example, in this study, we consider gradient aggregation. On the other hand, one open question is whether the proposed scheme can also be utilized for parameter aggregation. Based on our numerical tests, the performance (e.g., test accuracy) can be poor as the neural network may not be tolerant to the errors in the model parameters due to the proposed scheme. Hence, evaluating (and enhancing) the proposed scheme with a noise-tolerant neural network (e.g., quantized neural networks) along with various datasets is an interesting future research direction that can be pursued.

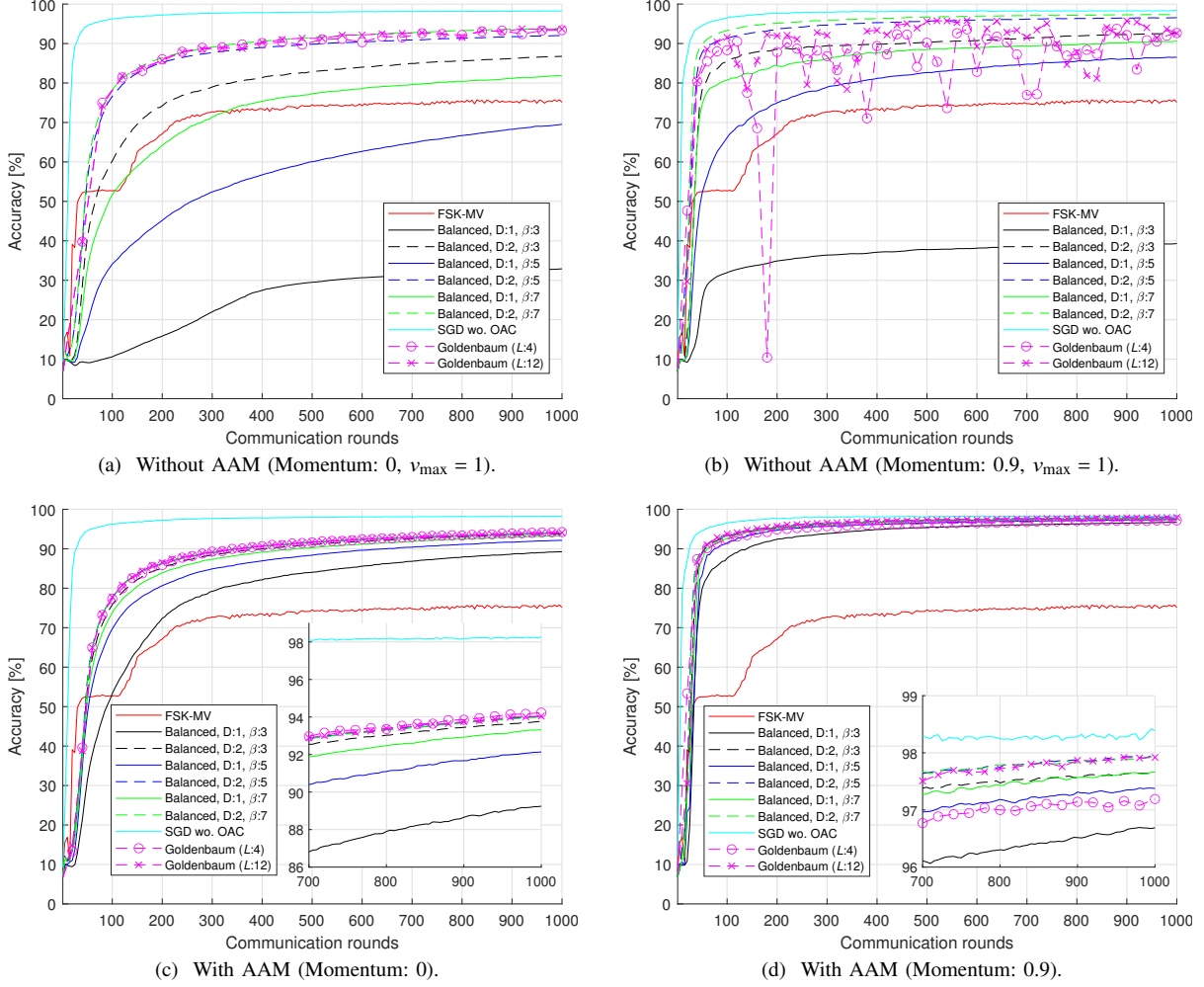


Fig. 8. Test accuracy versus communication rounds (Heterogeneous data distribution,  $R = 1$ ,  $K = 25$ ). The proposed scheme with AAM can provide a high test accuracy for a scenario with heterogeneous data distribution.

#### APPENDIX A DERIVATION OF (24)

The parameter  $\sigma_{\text{channel}}^2$  can be derived as

$$\begin{aligned}
 \sigma_{\text{channel}}^2 &\triangleq \mathbb{E}_{\bar{v}_q^{(\ell)}} \left[ \left( \hat{v}_q^{(\ell)} - \bar{v}_q^{(\ell)} \right)^2 \right] \\
 &\stackrel{(a)}{=} \mathbb{E}_{\bar{v}_q^{(\ell)}} \left[ \frac{v_{\max}^2}{\xi^2 R K^2} \sum_{i=0}^{D-1} \sum_{\ell=0}^{\beta-2} a_{\ell}^2 \left( K_{q,i,\ell} + \frac{\sigma_n^2}{E_s} \right)^2 \beta^{2i} \right] \\
 &\stackrel{(b)}{=} \frac{v_{\max}^2}{\xi^2 R K^2} \sum_{i=0}^{D-1} \sum_{\ell=0}^{\beta-2} a_{\ell}^2 \mathbb{E}_{K_{q,i,\ell}} \left[ \left( K_{q,i,\ell} + \frac{\sigma_n^2}{E_s} \right)^2 \right] \beta^{2i} \\
 &\stackrel{(c)}{=} \frac{v_{\max}^2}{R} \left( \frac{1}{3\beta} + \frac{1}{K} \left( \frac{\beta-1}{3\beta} + \frac{2\sigma_n^2}{3E_s} \right) + \frac{\beta\sigma_n^4}{3K^2 E_s^2} \right) \frac{\beta^D + 1}{\beta^D - 1}, \\
 &\stackrel{(d)}{=} v_{\max}^2 \frac{1}{3R} \left( \frac{1}{\beta} \left( 1 + \frac{\beta\sigma_n^2}{K(\beta-1)} \right)^2 + \frac{\beta}{K(\beta-1)} \right) \frac{\beta^D + 1}{\beta^D - 1},
 \end{aligned}$$

where (a) is from (23), (b) is because the distribution of  $K_{q,i,\ell}$  is  $\mathcal{B}(K, 1/\beta)$  when the distribution of  $\tilde{g}_{k,q}^{(\ell)}$  is  $\mathcal{U}(-v'_{\max}, v'_{\max})$ ,

(c) is because of the relation given by

$$\begin{aligned}
 &\mathbb{E}_{K_{q,i,\ell}} \left[ \left( K_{q,i,\ell} + \frac{\sigma_n^2}{E_s} \right)^2 \right] \\
 &= \mathbb{E}_{K_{q,i,\ell}} \left[ K_{q,i,\ell}^2 \right] + 2 \frac{\sigma_n^2}{E_s} \mathbb{E}_{K_{q,i,\ell}} \left[ K_{q,i,\ell} \right] + \frac{\sigma_n^4}{E_s^2} \\
 &= \frac{K^2}{\beta^2} + \frac{K(\beta-1)}{\beta^2} + 2 \frac{\sigma_n^2}{E_s} \frac{K}{\beta} + \frac{\sigma_n^4}{E_s^2} \\
 &= \frac{K^2}{\beta^2} + K \left( \frac{\beta-1}{\beta^2} + \frac{2\sigma_n^2}{\beta E_s} \right) + \frac{\sigma_n^4}{E_s^2}, \tag{31}
 \end{aligned}$$

and the identities given by

$$\begin{aligned}
 \frac{1}{\xi^2} \sum_{i=0}^{D-1} \beta^{2i} &= \frac{1}{\xi^2} \frac{\beta^{2D} - 1}{\beta^2 - 1} = \frac{4}{\beta^2 - 1} \frac{\beta^D + 1}{\beta^D - 1}, \\
 \sum_{\ell=0}^{\beta-2} a_{\ell}^2 &= \sum_{\ell=0}^{\frac{\beta-1}{2}} \ell^2 = \frac{(\beta-1)\beta(\beta+1)}{12},
 \end{aligned}$$

for  $\xi \triangleq (\beta^D - 1)/2$ , and (d) is because of  $E_s = \beta - 1$  as discussed in Section III-B.

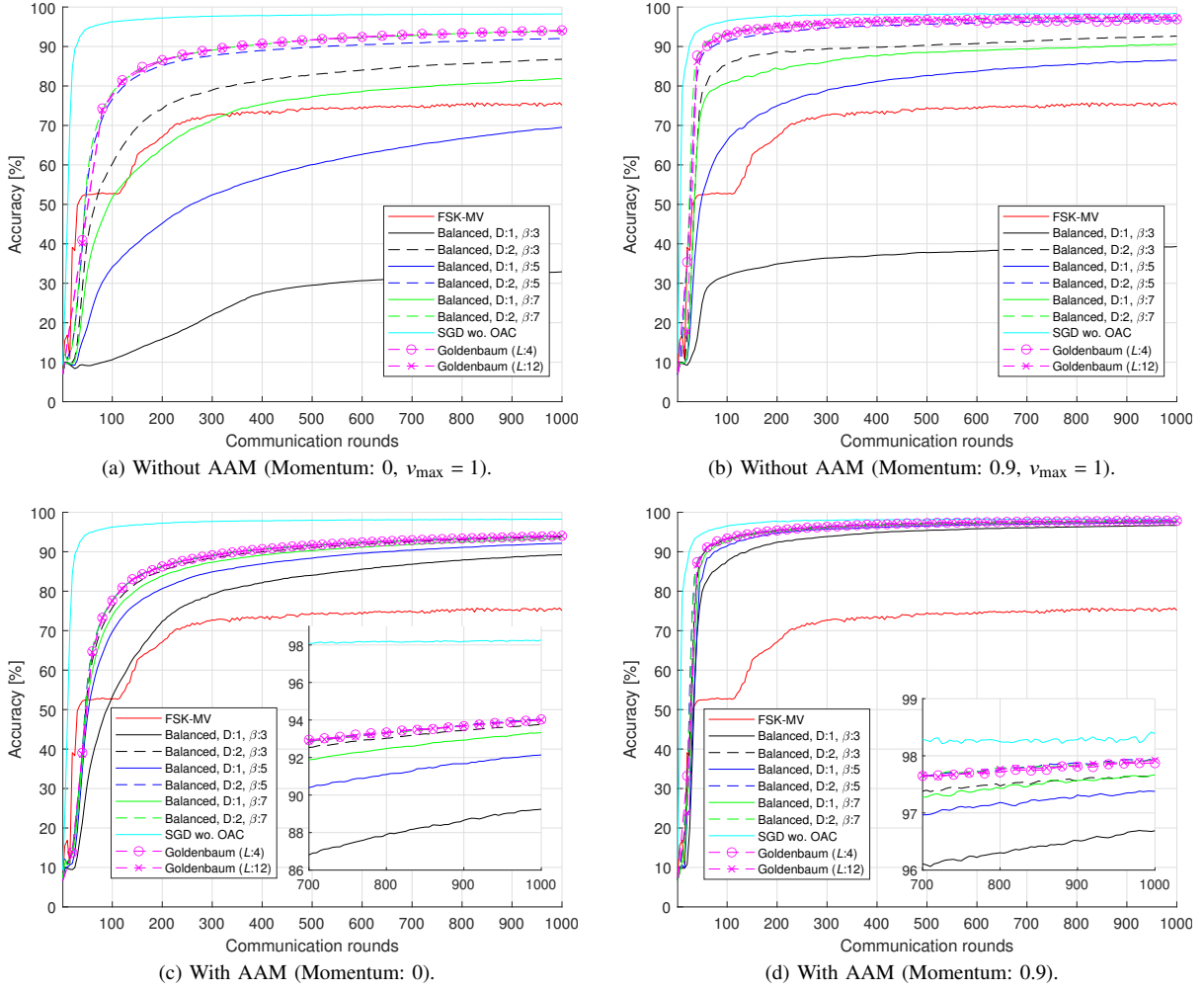


Fig. 9. Test accuracy versus communication rounds (Heterogeneous data distribution,  $R = 25$ ,  $K = 25$ ).

## APPENDIX B PROOF OF THEOREM 1

*Proof.* By Assumption 2, we utilize Lemma 1 to obtain the following inequality:

$$F(\mathbf{w}^{(\ell+1)}) - F(\mathbf{w}^{(\ell)}) \leq -\eta \mathbf{g}^{(\ell)\top} \hat{\mathbf{v}}^{(\ell)} + \frac{\eta^2 L}{2} \|\hat{\mathbf{v}}^{(\ell)}\|_2^2,$$

for  $\mathbf{w}^{(\ell+1)} = \mathbf{w}^{(\ell)} - \eta \hat{\mathbf{v}}^{(\ell)}$ . By using Assumptions 3 and Assumption 5, we obtain

$$\mathbb{E} \left[ \mathbf{g}^{(\ell)\top} \hat{\mathbf{v}}^{(\ell)} \right] = \mathbf{g}^{(\ell)\top} \left( \mathbb{E} \left[ \mathbf{v}^{(\ell)} + \mathbf{b}^{(\ell)} + \mathbf{c}^{(\ell)} \right] \right) = \|\mathbf{g}^{(\ell)}\|_2^2.$$

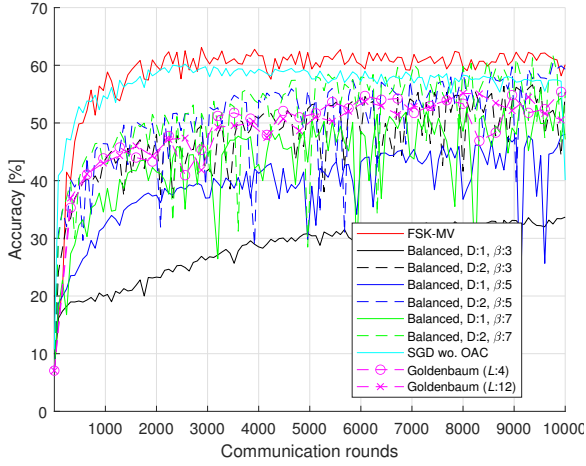
By using Assumptions 4-6, we can also obtain

$$\begin{aligned} \mathbb{E} \left[ \|\hat{\mathbf{v}}^{(\ell)}\|_2^2 \right] &= \mathbb{E} \left[ \left\| \mathbb{E} \left[ \hat{\mathbf{v}}^{(\ell)} \right] \right\|_2^2 \right] + \mathbb{E} \left[ \left\| \hat{\mathbf{v}}^{(\ell)} - \mathbb{E} \left[ \hat{\mathbf{v}}^{(\ell)} \right] \right\|_2^2 \right] \\ &= \underbrace{\|\mathbf{g}^{(\ell)}\|_2^2 + \mathbb{E} \left[ \|\hat{\mathbf{v}}^{(\ell)} - \mathbf{v}^{(\ell)}\|_2^2 \right]}_{\leq (\sigma_{\text{channel}}^2 + \sigma_{\text{quan}}^2) Q} + \underbrace{\mathbb{E} \left[ \|\mathbf{v}^{(\ell)} - \mathbf{g}^{(\ell)}\|_2^2 \right]}_{\leq \frac{1}{K} \sum_{k=0}^{K-1} \delta_k}. \end{aligned} \quad (32)$$

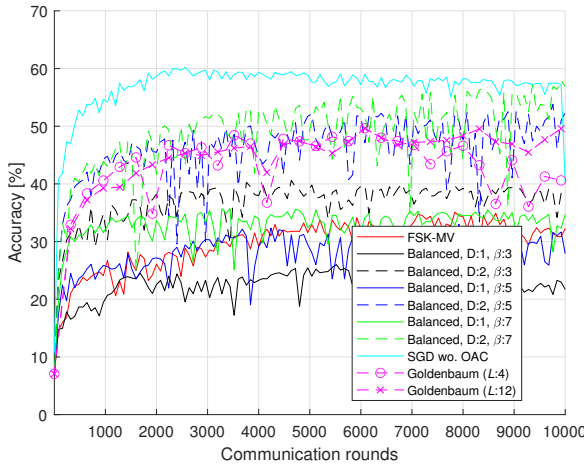
Therefore, for a given  $\mathbf{w}^{(\ell)}$ , the expected improvement can be expressed as

$$\begin{aligned} \mathbb{E} \left[ F(\mathbf{w}^{(\ell+1)}) - F(\mathbf{w}^{(\ell)}) \right] &= -\eta \mathbf{g}^{(\ell)\top} \mathbb{E} \left[ \hat{\mathbf{v}}^{(\ell)} \right] + \frac{\eta^2 L}{2} \mathbb{E} \left[ \|\hat{\mathbf{v}}^{(\ell)}\|_2^2 \right] \\ &\leq -\eta \|\mathbf{g}^{(\ell)}\|_2^2 + \frac{\eta^2 L}{2} \left( \|\mathbf{g}^{(\ell)}\|_2^2 + (\sigma_{\text{channel}}^2 + \sigma_{\text{quan}}^2) Q + \frac{1}{K} \sum_{k=0}^{K-1} \delta_k \right). \end{aligned}$$

By using Assumption 1, we perform a telescoping sum over the iterations and calculate the expectation over the random-



(a) Homogeneous data distribution.



(b) Heterogeneous data distribution.

Fig. 10. Test accuracy versus communication rounds for CIFAR10 dataset ( $R = 1$ , momentum: 0, AAM is enabled).

ness in the trajectory as

$$\begin{aligned}
F(\mathbf{w}^{(0)}) - F^* &\geq F(\mathbf{w}^{(0)}) - \mathbb{E} \left[ F(\mathbf{w}^{(T)}) \right] \\
&= \mathbb{E} \left[ \sum_{\ell=0}^{T-1} F(\mathbf{w}^{(\ell)}) - F(\mathbf{w}^{(\ell+1)}) \right] \\
&\geq \sum_{\ell=0}^{T-1} \mathbb{E} \left[ F(\mathbf{w}^{(\ell)}) - F(\mathbf{w}^{(\ell+1)}) \right] \\
&\geq \left( -\eta + \frac{\eta^2 L}{2} \right) \mathbb{E} \left[ \sum_{\ell=0}^{T-1} \|\mathbf{g}^{(\ell)}\|_2^2 \right] \\
&\quad + \frac{\eta^2 L T}{2} \left( (\sigma_{\text{channel}}^2 + \sigma_{\text{quan}}^2) Q + \frac{1}{K} \sum_{k=0}^{K-1} \delta_k \right).
\end{aligned}$$

By rearranging the terms, (29) is reached.  $\square$

#### APPENDIX C PROOF OF THEOREM 2

*Proof.* The proof of Theorem 2 is similar to that of Theorem 1. We re-evaluate  $\mathbb{E} \left[ \|\hat{\mathbf{v}}^{(\ell)} - \mathbf{v}^{(\ell)}\|_2^2 \right]$  in (32) under AAM. To this

end, let  $\mathbf{a}_k^{(\ell)} \triangleq \mathbb{E} \left[ \tilde{\mathbf{g}}_k^{(\ell)} - \mathbf{g}^{(\ell)} \right]$  be the bias vector due to data heterogeneity. Based on Assumption 4,

$$\begin{aligned}
\mathbb{E} \left[ \|\tilde{\mathbf{g}}_k^{(\ell)}\|_2^2 \right] &= \mathbb{E} \left[ \|\tilde{\mathbf{g}}_k^{(\ell)} - \mathbf{g}^{(\ell)}\|_2^2 \right] - \|\mathbf{g}^{(\ell)}\|_2^2 - 2\mathbf{g}^{(\ell)\top} \mathbf{a}_k^{(\ell)} \\
&\leq \delta_k + \|\mathbf{g}^{(\ell)}\|_2^2 + 2\mathbf{g}^{(\ell)\top} \mathbf{a}_k^{(\ell)}. \tag{33}
\end{aligned}$$

Therefore, based on (27), (33), and by Assumption 3,

$$\begin{aligned}
\mathbb{E}_{\hat{\mathbf{v}}^{(\ell)}} \left[ \|\hat{\mathbf{v}}^{(\ell)} - \mathbf{v}^{(\ell)}\|_2^2 \right] &= E_{\text{total}} \mathbb{E}_{\{\tilde{\mathbf{g}}_k^{(\ell-1)}\}} \left[ v_{\text{max}}^{(\ell)2} \right] \\
&= \alpha^2 E_{\text{total}} \mathbb{E}_{\{\tilde{\mathbf{g}}_k^{(\ell-1)}\}} \left[ \|\mathbf{m}^{(\ell-1)}\|_\infty^2 \right] \\
&\leq \alpha^2 E_{\text{total}} \mathbb{E}_{\{\tilde{\mathbf{g}}_k^{(\ell-1)}\}} \left[ \|\mathbf{m}^{(\ell-1)}\|_2^2 \right] \\
&= \alpha^2 E_{\text{total}} \mathbb{E}_{\{\tilde{\mathbf{g}}_k^{(\ell-1)}\}} \left[ \sum_{k=0}^{K-1} \|\tilde{\mathbf{g}}_k^{(\ell-1)}\|_2^2 \right] \\
&= \alpha^2 E_{\text{total}} \sum_{k=0}^{K-1} \mathbb{E}_{\tilde{\mathbf{g}}_k^{(\ell-1)}} \left[ \|\tilde{\mathbf{g}}_k^{(\ell-1)}\|_2^2 \right] \\
&\leq \alpha^2 E_{\text{total}} \left( K \|\mathbf{g}^{(\ell-1)}\|_2^2 + \sum_{k=0}^{K-1} \delta_k + 2\mathbf{g}^{(\ell-1)\top} \underbrace{\sum_{k=0}^{K-1} \mathbf{a}_k^{(\ell-1)}}_{=0} \right).
\end{aligned}$$

Therefore, the expected improvement given in Appendix B with AAM can be re-expressed as

$$\begin{aligned}
\mathbb{E} \left[ F(\mathbf{w}^{(\ell+1)}) - F(\mathbf{w}^{(\ell)}) \right] &= -\eta \mathbf{g}^{(\ell)\top} \mathbb{E} \left[ \hat{\mathbf{v}}^{(\ell)} \right] + \frac{\eta^2 L}{2} \mathbb{E} \left[ \|\hat{\mathbf{v}}^{(\ell)}\|_2^2 \right] \\
&\leq \left( -\eta + \frac{\eta^2 L}{2} \right) \|\mathbf{g}^{(\ell)}\|_2^2 + \frac{\eta^2 L}{2} \alpha^2 E_{\text{total}} K \|\mathbf{g}^{(\ell-1)}\|_2^2 \\
&\quad + \frac{\eta^2 L}{2} (\alpha^2 E_{\text{total}} K + 1) \frac{1}{K} \sum_{k=0}^{K-1} \delta_k.
\end{aligned}$$

Considering Assumption 1, we perform a telescoping sum over the iterations and calculate the expectation over the randomness in the trajectory as

$$\begin{aligned}
F(\mathbf{w}^{(1)}) - F^* &\geq \sum_{\ell=0}^{T-1} \mathbb{E} \left[ F(\mathbf{w}^{(\ell)}) - F(\mathbf{w}^{(\ell+1)}) \right] \\
&\geq \left( -\eta + \frac{\eta^2 L}{2} \right) \mathbb{E} \left[ \sum_{\ell=1}^T \|\mathbf{g}^{(\ell)}\|_2^2 \right] \\
&\quad + \frac{\eta^2 L}{2} \alpha^2 E_{\text{total}} K \mathbb{E} \left[ \sum_{\ell=1}^T \|\mathbf{g}^{(\ell-1)}\|_2^2 \right] \\
&\quad + \frac{\eta^2 L T}{2} (\alpha^2 E_{\text{total}} K + 1) \frac{1}{K} \sum_{k=0}^{K-1} \delta_k. \tag{34}
\end{aligned}$$

Also, we can express the expected value of the sum over the trajectory as

$$\mathbb{E} \left[ \sum_{\ell=1}^T \|\mathbf{g}^{(\ell-1)}\|_2^2 \right] = \mathbb{E} \left[ \sum_{\ell=1}^T \|\mathbf{g}^{(\ell)}\|_2^2 \right] + \mathbb{E} \left[ \|\mathbf{g}^{(0)}\|_2^2 - \|\mathbf{g}^{(T)}\|_2^2 \right]. \tag{35}$$

Finally, by using (35) and rearranging the terms in (34), (29) is obtained.  $\square$

## REFERENCES

- [1] A. Şahin and R. Yang, "Over-the-air computation over balanced numerals," in *Proc. IEEE Global Communication Conference (GLOBECOM) - Workshop on Wireless Communications for Distributed Intelligence*, Dec. 2022, pp. 1–6.
- [2] B. Nazer and M. Gastpar, "Computation over multiple-access channels," *IEEE Trans. Inf. Theory*, vol. 53, no. 10, pp. 3498–3516, Oct. 2007.
- [3] M. Gastpar and M. Vetterli, "Source-channel communication in sensor networks," in *Proc. International Conference on Information Processing in Sensor Networks*, ser. IPSN'03. Berlin, Heidelberg: Springer-Verlag, 2003, p. 162–177.
- [4] M. Goldenbaum, H. Boche, and S. Stańczak, "Harnessing interference for analog function computation in wireless sensor networks," *IEEE Trans. Signal Process.*, vol. 61, no. 20, pp. 4893–4906, Oct. 2013.
- [5] W. Liu, X. Zang, Y. Li, and B. Vucetic, "Over-the-air computation systems: Optimization, analysis and scaling laws," *IEEE Trans. Wireless Commun.*, vol. 19, no. 8, pp. 5488–5502, Aug. 2020.
- [6] M. Chen, D. Gündüz, K. Huang, W. Saad, M. Bennis, A. V. Feljan, and H. Vincent Poor, "Distributed learning in wireless networks: Recent progress and future challenges," *IEEE J. Sel. Areas Commun.*, pp. 1–26, 2021.
- [7] P. Park, P. Di Marco, and C. Fischione, "Optimized over-the-air computation for wireless control systems," *IEEE Commun. Lett.*, vol. 26, no. 2, pp. 1–5, 2022.
- [8] B. McMahan, E. Moore, D. Ramage, S. Hampson, and B. A. y. Arcas, "Communication-Efficient Learning of Deep Networks from Decentralized Data," in *Proc. International Conference on Artificial Intelligence and Statistics*, ser. Proceedings of Machine Learning Research, A. Singh and J. Zhu, Eds., vol. 54. PMLR, 20–22 Apr 2017, pp. 1273–1282.
- [9] M. Chen, Z. Yang, W. Saad, C. Yin, H. V. Poor, and S. Cui, "A joint learning and communications framework for federated learning over wireless networks," *IEEE Trans. Wireless Commun.*, vol. 20, no. 1, pp. 269–283, 2021.
- [10] G. Zhu, Y. Wang, and K. Huang, "Broadband analog aggregation for low-latency federated edge learning," *IEEE Trans. Wireless Commun.*, vol. 19, no. 1, pp. 491–506, Jan. 2020.
- [11] T. Sery, N. Shlezinger, K. Cohen, and Y. C. Eldar, "Over-the-air federated learning from heterogeneous data," *IEEE Transactions on Signal Processing*, vol. 69, pp. 3796–3811, 2021.
- [12] M. M. Amiri and D. Gündüz, "Federated learning over wireless fading channels," *IEEE Trans. Wireless Commun.*, vol. 19, no. 5, pp. 3546–3557, Feb. 2020.
- [13] G. Zhu, Y. Du, D. Gündüz, and K. Huang, "One-bit over-the-air aggregation for communication-efficient federated edge learning: Design and convergence analysis," *IEEE Trans. Wireless Commun.*, vol. 20, no. 3, pp. 2120–2135, Nov. 2021.
- [14] N. Zhang and M. Tao, "Gradient statistics aware power control for over-the-air federated learning," *IEEE Trans. Wireless Commun.*, vol. 20, no. 8, pp. 5115–5128, 2021.
- [15] H. Hellström, V. Fodor, and C. Fischione, "Over-the-air federated learning with retransmissions," in *Proc. IEEE International Workshop on Signal Processing Advances in Wireless Communications (SPAWC)*, 2021, pp. 291–295.
- [16] L. Su and V. K. N. Lau, "Hierarchical federated learning for hybrid data partitioning across multitype sensors," *IEEE Internet of Things Journal*, vol. 8, no. 13, pp. 10922–10939, Jan. 2021.
- [17] X. Zang, W. Liu, Y. Li, and B. Vucetic, "Over-the-air computation systems: Optimal design with sum-power constraint," *IEEE Wireless Commun. Lett.*, vol. 9, no. 9, pp. 1524–1528, 2020.
- [18] M. A. Abdul Careem and A. Dutta, "Real-time prediction of non-stationary wireless channels," *IEEE Trans. Wireless Commun.*, vol. 19, no. 12, pp. 7836–7850, 2020.
- [19] H. Jung and S.-W. Ko, "Performance analysis of UAV-enabled over-the-air computation under imperfect channel estimation," *IEEE Wireless Commun. Lett.*, pp. 1–1, Nov. 2021.
- [20] M. Goldenbaum and S. Stańczak, "Robust analog function computation via wireless multiple-access channels," *IEEE Trans. Commun.*, vol. 61, no. 9, pp. 3863–3877, 2013.
- [21] —, "Computing the geometric mean over multiple-access channels: Error analysis and comparisons," in *IEEE Asilomar Conference on Signals, Systems and Computers*, 2010, pp. 2172–2178.
- [22] A. Şahin, "Distributed learning over a wireless network with non-coherent majority vote computation," *IEEE Trans. Wireless Commun.*, pp. 1–16, 2023.
- [23] I. Koren, *Computer Arithmetic Algorithms*, 2nd ed. A K Peters/CRC Press, 2018.
- [24] J. Bernstein, Y.-X. Wang, K. Azizzadenesheli, and A. Anandkumar, "signSGD: Compressed optimisation for non-convex problems," in *Proc. International Conference on Machine Learning*, vol. 80. Proceedings of Machine Learning Research, 10–15 Jul 2018, pp. 560–569.
- [25] R. Jiang and S. Zhou, "Cluster-based cooperative digital over-the-air aggregation for wireless federated edge learning," in *IEEE/CIC International Conference on Communications in China (ICCC)*, 2020, pp. 887–892.
- [26] B. Chen, R. Jiang, T. Kasetkasem, and P. Varshney, "Channel aware decision fusion in wireless sensor networks," *IEEE Transactions on Signal Processing*, vol. 52, no. 12, pp. 3454–3458, 2004.
- [27] A. Şahin, "A demonstration of over-the-air computation for federated edge learning," in *IEEE Globecom Workshops (GC Wkshps)*, 2022, pp. 1821–1827.
- [28] A. Şahin and R. Yang, "A survey on over-the-air computation," *IEEE Communications Surveys & Tutorials*, pp. 1–33, 2023.
- [29] X. Wei, C. Shen, H. J. Yang, and H. V. Poor, "Random orthogonalization for federated learning in massive MIMO systems," in *Proc. IEEE International Conference on Communications (ICC)*, Apr. 2022, pp. 1–6.
- [30] M. M. Amiria, T. M. Duman, D. Gündüz, S. R. Kulkarni, and H. Vincent Poor, "Collaborative machine learning at the wireless edge with blind transmitters," *IEEE Trans. Wireless Commun.*, pp. 1–1, Mar 2021.
- [31] A. Şahin, B. Everette, and S. Hoque, "Distributed learning over a wireless network with FSK-based majority vote," in *Proc. IEEE International Conference on Advanced Communication Technologies and Networking (CommNet)*, Dec. 2021, pp. 1–9.
- [32] —, "Over-the-air computation with DFT-spread OFDM for federated edge learning," in *Proc. IEEE Wireless Communications and Networking Conference (WCNC)*, Apr. 2022, pp. 1–6.
- [33] S. Hoque, M. H. Adeli, and A. Şahin, "Chirp-based over-the-air computation for long-range federated edge learning," in *Proc. IEEE International Symposium on Personal, Indoor and Mobile Radio Communications (PIMRC)*, Sep. 2022, pp. 1–7.
- [34] M. Goldenbaum and S. Stańczak, "On the channel estimation effort for analog computation over wireless multiple-access channels," *IEEE Wireless Commun. Lett.*, vol. 3, no. 3, pp. 261–264, 2014.
- [35] D. Alistarh, D. Grubic, J. Z. Li, R. Tomioka, and M. Vojnovic, "QSGD: Communication-efficient SGD via gradient quantization and encoding," in *Proc. International Conference on Neural Information Processing Systems (NeurIPS)*, ser. NIPS'17. Red Hook, NY, USA: Curran Associates Inc., 2017, pp. 1707–1718.
- [36] J. Xu, W. Du, Y. Jin, W. He, and R. Cheng, "Ternary compression for communication-efficient federated learning," *IEEE Transactions on Neural Networks and Learning Systems*, pp. 1–15, 2020.
- [37] M. Kim, W. Saad, M. Mozaffari, and M. Debbah, "On the tradeoff between energy, precision, and accuracy in federated quantized neural networks," in *Proc. IEEE International Conference on Communications (ICC)*, 2022, pp. 2194–2199.
- [38] K. Liang, H. Zhong, H. Chen, and Y. Wu, "Wyner-Ziv gradient compression for federated learning," 2021. [Online]. Available: <https://arxiv.org/abs/2111.08277>
- [39] E. Dahlman, S. Parkvall, and J. Skold, *5G NR: The Next Generation Wireless Access Technology*, 1st ed. USA: Academic Press, Inc., 2018.
- [40] O. Abari, H. Rahul, D. Katabi, and M. Pant, "AirShare: Distributed coherent transmission made seamless," in *Proc. IEEE Conference on Computer Communications (INFOCOM)*, 2015, pp. 1742–1750.
- [41] P. Liu, J. Jiang, G. Zhu, L. Cheng, W. Jiang, W. Luo, Y. Du, and Z. Wang, "Training time minimization for federated edge learning with optimized gradient quantization and bandwidth allocation," *Springer Frontiers of Information Technology & Electronic Engineering*, vol. 22, no. 8, pp. 2095–29230, 2022.
- [42] G. H. Hardy and E. M. Wright, *An Introduction to the Theory of Numbers*, 6th ed. Oxford, 2008.
- [43] Y. Nesterov, *Introductory Lectures on Convex Optimization: A Basic Course*, ser. Mathematics and its applications. Kluwer Academic Publishers, 2004.